

The response of a turbulent boundary layer to a step change in surface roughness

Part 1. Smooth to rough

By R. A. ANTONIA AND R. E. LUXTON

Department of Mechanical Engineering, University of Sydney

(Received 5 January 1970 and in revised form 30 November 1970)

The structure and growth of the internal boundary layer which forms downstream of a sudden change from a smooth to a rough surface under zero pressure gradient conditions has been studied experimentally. To keep pressure disturbances due to the roughness change small, the level of the rough surface was depressed, so that the crest of the roughness was aligned with the level of the smooth surface. It has been found that, in the region near the change, the structure of the internal layer is largely independent of that in the almost undisturbed outer layer, whilst both the zero time delay and the moving axis integral length scales in the internal layer are significantly reduced below those on the smooth wall. The growth-rate of the internal layer is similar to that of the zero pressure gradient boundary layer, whilst the level of turbulence inside the internal layer is high because of the large turbulent energy production near the rough wall. From the mixing length results, and an analysis of the turbulent energy equation, it is deduced that the internal layer flow near the wall is not in energy equilibrium, and hence the concept of inner layer similarity breaks down. From an initially self-preserving state on the smooth wall, the turbulent boundary layer approaches a second self-preserving state on the rough wall well downstream of the roughness step.

1. Introduction

The changes which occur in a turbulent boundary layer following a sudden perturbation from a self-preserving state have been the subject of several experimental and theoretical investigations. The majority of this work has been reviewed by Tani (1968). Both perturbations applied at the wall (as discontinuities in surface conditions) and perturbations applied to the free stream as step changes in pressure gradient have been studied. Of the investigations of the first type of perturbation, most have been concerned with the response of a turbulent boundary layer to a step change in surface roughness, perhaps because of the importance of this problem in micrometeorology.

The existing theories and calculation methods for the flow downstream of a change in roughness (e.g. Elliott 1958; Panofsky & Townsend 1964; Townsend 1965, 1966; Bradshaw, Ferriss & Atwell 1967; Taylor 1969) effectively require that the thickness of the perturbed flow region, or internal layer, is small compared with an overall length scale of the boundary layer. These theories are,

therefore, reasonably applicable in the atmospheric boundary layer for a limited distance downstream from the step change. Measurements by Bradley (1965) are typical of those in this region of the atmospheric boundary layer. There have also been some wind-tunnel investigations of a turbulent shear flow following a smooth-to-rough change (Jacobs 1939; Clauser 1956; Logan & Jones 1963; Plate & Hidy 1967; Makita 1968; Antonia & Luxton 1971 *a*) and following a rough-to-smooth change in surface (Jacobs 1939; Taylor 1962; Makita 1968), but it is unlikely that the above prediction methods would be applicable to these experiments, as in all cases the internal layer represents a significant fraction of the total boundary-layer thickness.

In his review of the information provided by the above experiments, Tani (1968) has concluded that the flow near the wall readjusts rapidly to the new surface condition, but that the wall shear stress downstream from the step† overshoots before slowly returning to its equilibrium value. Although this latter conclusion appears to be qualitatively supported by the available measurements, there is a need for accurate quantitative measurements of wall shear stress in the region immediately downstream from the step. In the experiments referenced above, the wall shear stress was inferred either from extrapolation of measurements of the Reynolds shear stress $-\overline{uv}$, or from the slope of an assumed semi-logarithmic velocity distribution. The accuracy of $-\overline{uv}$ measurements close to a wall is usually not good, and as extrapolation involves effectively a differentiation of the data, one cannot expect that an accurate skin-friction coefficient c_f could result from this technique. For the rough-to-smooth change, the Clauser chart method for determining c_f appears at first sight to be attractive, but an independent measurement of wall shear stress is needed to establish the universality of the constants involved. Estimation of c_f on a rough wall is a much more difficult matter. Even for a self-preserving boundary layer (Perry, Schofield & Joubert 1969), it is necessary to know the effective position of the wall and the value of a roughness function, or 'slip' velocity $\Delta U/U_r$, before the skin-friction coefficient can be determined. In the non-equilibrium flow close to a step change in roughness, the basis of this technique becomes suspect, and in any case both the effective origin and the roughness function are likely to be functions of stream-wise position.

Many workers have advanced the existence of a logarithmic mean velocity distribution in the region near the wall as evidence that the layer immediately downstream of the surface change is an equilibrium layer (in the sense described by Townsend 1961).

All the theories mentioned above effectively make this assumption, but no direct experimental evidence of equilibrium is yet available.

Of the experimental studies referred to above, only those by Logan & Jones (1963) in a pipe, and Makita (1968) in a channel, report measurements of the turbulence intensities and the turbulence shear stress. These experiments may be expected to provide a reasonably complete picture of the readjustment of the flow following the surface change, but this picture is complicated by the sudden

† For convenience, 'step' is used to mean 'step change in roughness' here and in other places throughout the text.

change in pressure gradient which accompanies the roughness change in fully developed internal flows. To date, there has been no satisfactory experimental study reported of the response of a zero pressure gradient turbulent boundary layer to a change in surface roughness.

Antonia & Luxton (1971*a*) investigated the flow field downstream of an upstanding† change in surface roughness. From a limited number of turbulence measurements, it was deduced that in the region near the change the structure of the internal layer was largely independent of that in the undisturbed outer layer, whilst the integral length scales in the internal layer were significantly reduced below those on the smooth wall. It was found, however, that the disturbance introduced by the first roughness element had a significant effect on the flow immediately downstream. In order to minimize this disturbance, the level of the rough surface has for the present experiments been depressed below that of the smooth wall, so that the crest of the roughness is now aligned with the level of the smooth surface. One of the aims of the present study is to verify the above deductions for the new surface configuration. Particular attention is given to the structure and growth of the internal layer downstream of the step and to the mean flow velocity distributions (§5).

The variation of the wall shear stress in the region near the step is deduced from the measurements of profile drag obtained by pressure tapping the roughness elements. This variation is compared in §3 with that of the skin-friction coefficient inferred from the slope of the logarithmic mean velocity profiles. The conclusion drawn by Tani (1968), that the surface shear stress at first overshoots and then gradually falls to its final value, the whole readjustment to the new surface condition being quite rapid, is supported by the present wall shear stress measurements.

The rate of growth of the internal layer is discussed in §6, whilst the distributions of turbulence intensity are presented in §7. These results show that the edge of the internal layer grows at a rate similar to that of the zero pressure gradient boundary layer, whilst the level of the turbulence inside the internal layer is high because of the large turbulent energy production near the rough wall. From the mixing length results (§8) and the analyses of the turbulent energy equation (§9), it is deduced that the internal layer flow near the wall is not in energy equilibrium, and that inner layer similarity arguments are inapplicable. It is seen (§10) that both the zero time delay and moving axis length scales are significantly reduced as the flow enters the internal layer.

The approach of the turbulent boundary layer to a second self-preserving state is verified by the results of §4 and §7. These turbulence measurements in the self-preserving rough wall boundary layer are an essential starting point for the study of the response of a boundary layer to a rough-to-smooth change in surface (Antonia & Luxton 1969).

† In this investigation, the roughness elements were upstanding from the level of the upstream smooth surface, the face of the first element being totally exposed to the oncoming flow.

2. Experimental arrangement

The experimental boundary layer is formed on the floor of the working section of a moderately low-turbulence wind tunnel. The tunnel, which is of the open type, has a 9:1 contraction feeding a 15 in. wide by 9 in. high working section. The working section is 16 ft long, and has a variable roof geometry to permit adjustment of the pressure gradient. The experimental configuration being investigated consists of a smooth floor 8 ft long followed by a rough floor of similar length. The roughness is of the 'k-type',[†] and is the same geometry as that used by Moore (1951) and by Perry & Joubert (1963). It consists of rectangular slats of $\frac{1}{8}$ in. square cross-section and a pitch of $\frac{1}{2}$ in. The first roughness element is depressed below the smooth surface, the crest of the roughness being aligned with the smooth wall surface (figure 1). The slats span the entire width of the tunnel

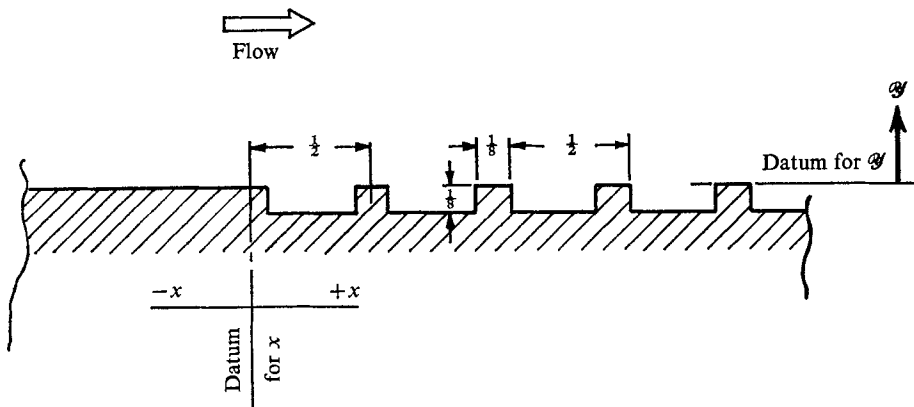


FIGURE 1. Geometry of surface and co-ordinate system.

and are faired into the corner fillets of the working section. The rough floor is made up of four timber panels and a 1 ft. long steel section which may be moved to almost any streamwise position. This section provides an accurately defined example of the roughness with elements located to within ± 0.001 in. It can also accommodate pressure-tapped elements for form drag measurements. The height of the elements on the timber sections is accurate to about ± 0.005 in.

Measurements have been made at values of U_1 , the free-stream velocity, of approximately $18 \text{ ft}^{-1} \text{ sec}$ and $33 \text{ ft}^{-1} \text{ sec}$, with a zero streamwise pressure gradient. With a $\frac{1}{8}$ in. diameter tripping rod spanning the working section about one foot downstream from the contraction, the boundary-layer thickness δ_s at the smooth-rough surface change is about 1.9 in. at the lower Reynolds number $U_1 \delta_s / \nu \simeq 1.9 \times 10^4$ and 1.8 in. at $U_1 \delta_s / \nu \simeq 3.1 \times 10^4$.

The majority of the mean velocity and turbulence intensity traverses were carried out normal to the wall and in the centre plane of the tunnel. The geometric centre of the measuring probe was usually located at the mid-point on the crest of

[†] A 'k-type' roughness is defined as one for which the roughness function $\Delta U/U_\tau$ (defined in §6 of the paper) scales on k , the physical height of the roughness.

a roughness element but a few traverses were made in between roughness elements. The mean velocity profiles for both tunnel speeds were obtained with a single hot wire (0.00012 in. dia. tungsten, 0.040 in. long) and a constant-temperature anemometer system designed by Fraser (1969). This was also used for measuring the u -component turbulence intensity. The mean velocity profiles at the higher tunnel speed were also obtained with a Pitot-static probe, used in conjunction with a Texas Model 145 Precision Pressure Gauge. The v -component turbulence intensity was obtained with a miniature DISA X -probe with 0.0002 in. dia. platinum coated tungsten wires, 0.040 in. long. The shear stress was measured with this X -probe and with a single rotating inclined hot wire.

All signals were recorded in digital form after passing through sharp 1 kHz low-pass filters. The digital records were then processed on the English Electric KDF 9 computer in the Basser Computing Department of the University of Sydney. Details of the digital data system may be found in Luxton, Swenson & Chadwick (1967).

The form drag results presented in §3 were obtained with a pressure tapped roughness element, which could be located at any desired position on the steel roughness section. The vertical faces of the steel element were drilled at various distances up to the height of the element. No pressure taps were inserted on the roughness crest. The pressure holes were approximately 0.016 in. in diameter and were spaced at regular intervals of 0.15 in. in the transverse direction. The holes were situated approximately on a straight line inclined at about 4° to the horizontal, and spanned a distance of about 1.20 in. across the tunnel floor. These sensing holes were connected to hypodermic tubes set into the base of the element.

The pressures were measured with the Texas Precision Pressure Gauge Model 145, used in the null mode, and sensitive to 0.01 mm of water. Frequent checks of these pressures were also made with a null reading Combist micromanometer of rather greater sensitivity (about 0.003 mm of water). The agreement between the two instruments was good but the Texas pressure transducer was found to be easier to read.

The space-time correlation measurements presented in §10 were obtained with the use of two single wires. The wires were made of 0.00012 in. dia. tungsten and were 0.040 in. long. The probes carrying these wires were mounted on separate traverse gears. The downstream traverse gear allowed accurate movements in the x , y and z directions. The transverse gear used for the upstream probe allowed accurate traversing in the y and z directions only. Most of the measurements presented here are for nominally zero separation of the wires in both the y and z directions. The wires used usually had fairly closely matched cold resistance values as they were chosen from a batch of wires which had been plated during the same process. The stings to which the wire ends were soldered were shaped to minimize the interference to the downstream stings. Also, the $\frac{1}{8}$ in. dia. stem of the downstream probe was at a distance of about 60 diameters from the stem (also of $\frac{1}{8}$ in. dia.) of the upstream probe at the position of zero x separation. This position was in general determined by eye, and an accuracy of no better than 0.010 in. can be claimed for the x direction. The zero y separation was found to be

more critical as a small relative y displacement had a significant effect on the correlation for small x separations. The zero y displacement setting was usually determined by comparing the oscilloscope traces of the wire signals. Although the results presented in § 10 were normalized with respect to the intensities at the two wire positions, the wires were usually calibrated for each series of experiments, and turbulence intensities could therefore be computed at a few points in the boundary layer to check that the wires were operating satisfactorily.

3. Determination of wall shear stress

As stated in § 1 the measurement of skin friction on a rough surface is difficult. An indirect method, known as the 'error in origin' method, was used with seeming success by Perry & Joubert (1963) for rough wall layers which are fully developed

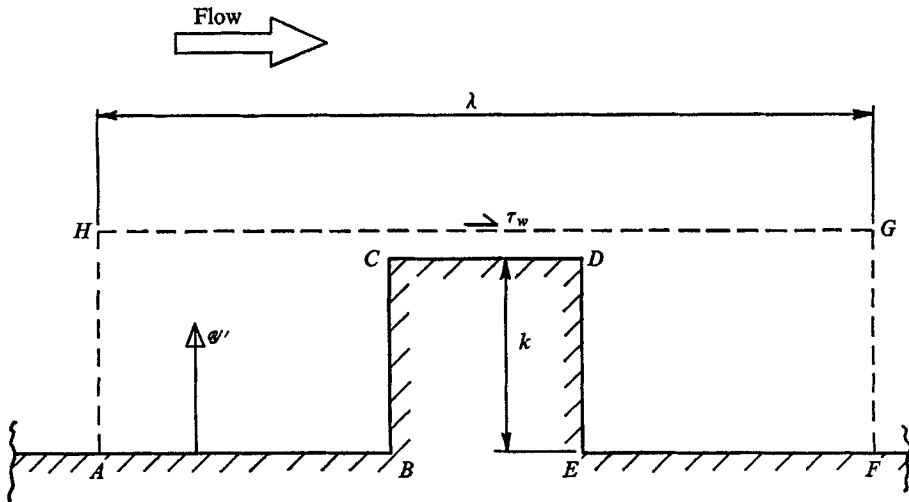


FIGURE 2. Control volume used in determination of effective wall shear stress τ_w .

and are likely to be in a state of energy equilibrium. In the present experiments, close to the change from the smooth to the rough surface, the rough wall layer is not fully developed and is unlikely to be in energy equilibrium. Accordingly, the indirect 'error in origin' method, which presumes the existence of a logarithmic region and effectively forces the measured profile into a logarithmic form by trial-and-error shifting of the origin, is unlikely to give reliable results. Two direct methods are available: the floating element skin-friction balance (which has been used successfully on smooth walls with small pressure gradients, and on a large scale rough surface, in the micrometeorological studies by Bradley (1965)), and the measurement of the form drag of individual roughness elements (as used recently by Perry *et al.* (1969), and by Antonia & Luxton (1971*a*)).

In the present work the form drag method has been used. As the theory of this method has been given in Perry *et al.* (1969) only points of question will be raised here. Referring to figure 2, the method assumes (i) the combined contribution to the momentum balance in the x direction due to the viscous shear stresses on

AB , CD and EF is negligible; (ii) the momentum efflux out of FG is equal to the momentum influx through HA ; (iii) the integrals of the pressure distributions over FG and HA are equal. The most questionable part of the first assumption is that the shear stress on the crest of the roughness element is small.

Surface flow visualization studies by Schofield (1969) on a comparable rough surface under fully developed conditions suggested the presence of a separation bubble affecting the early part of the flow on the roughness crest. Further, it is likely that in the cavities between elements reversed flow exists over the whole of EF and part of AB . As the shear stresses on these surfaces are also neglected it is possible that the combined neglect of stresses on CD , EF and AB results in small error. Nevertheless, reliable, independent measurements of the shear stress on the roughness crest would be useful. Assumptions (ii) and (iii) are difficult to test experimentally with roughness of the present scale as the introduction of a probe into the cavities between the elements is likely to disturb the flow in the cavities. However, the assumptions appear to be reasonable at least for elements not too close to the start of the roughness. A small streamwise pressure gradient could be detected near the crests of the first two or three roughness elements and it is likely that this also existed between the elements.

With the above assumptions the x -momentum balance reduces to

$$\tau_{HG}\lambda = \int_0^k (P_1 - P_2) dy', \quad (1)$$

where λ is the pitch of the roughness, P_1 and P_2 are the pressures on the front and rear faces of the roughness element, k is the height of the element and y' is measured from the base of the element. It must be noted that τ_{HG} is a measure of the momentum transport across the surface HG , and as such it has contributions from $\langle -\bar{w}\bar{v} \rangle$, $\langle \nu \partial U / \partial y \rangle$ and $\langle -UV \rangle$, where U and V are the values of the time mean streamwise and vertical velocities, and $\langle \rangle$ denotes the average over one pitch length λ . Thus, if there is a periodic mean flow field induced by the periodic roughness, and there is a phase difference between U and V , there will be a contribution to τ_{HG} due to mean flow momentum transport. The importance of this term cannot be assessed for the present but measurements of $\bar{w}\bar{v}$ presented in §7 suggest that it may be significant if HG is taken close to the crest of the roughness.

At the lower of the two Reynolds numbers the pressure difference ($P_1 - P_2$) across a roughness element was small and consequently the accuracy of measurement was poor. For this reason, most of the measurements presented in §3 were made at $U_1 \delta_s / \nu \simeq 3.1 \times 10^4$. The reproducibility of these profiles was good, but even at the higher Reynolds number the minimum difference recorded (approximately half way up the element) was only about 0.1 mm of water, and a resolution error of up to 13% is possible for this value. The pressures P_1 and P_2 were measured relative to the pressure at a hole near the crest of the trailing face of the element. Very little variation was found for the distribution of P_2 , and for this reason only the pressure difference ($P_1 - P_2$) is shown in figure 3 plotted against y'/k . It is seen in figure 3 that the pressure distribution rises near the crest and near the base of the roughness, and has a broad minimum in the region of $y'/k = 0.5$.

The distribution is not symmetrical about the mid-height, as the pressure rise near the crest is greater than that near the base. This asymmetry persisted to the last measuring station at $x = 46.5$ in. (figure 4), and was evident at both Reynolds numbers. It must also be remarked that the spatial resolution of the pressures plotted in figures 3 and 4 is not good, owing to the unavoidably large diameter of the measuring holes in comparison with the element height. In particular, the shape of the distribution near the crest and near the base of the element is poorly defined. It may be noted that no evidence of a stagnation line on the leading face of an element may be seen, nor was there any evidence of stagnation in the flow-visualization experiments of Liu, Kline & Johnston (1966) and of Schofield (1969), both for comparable roughness geometries.

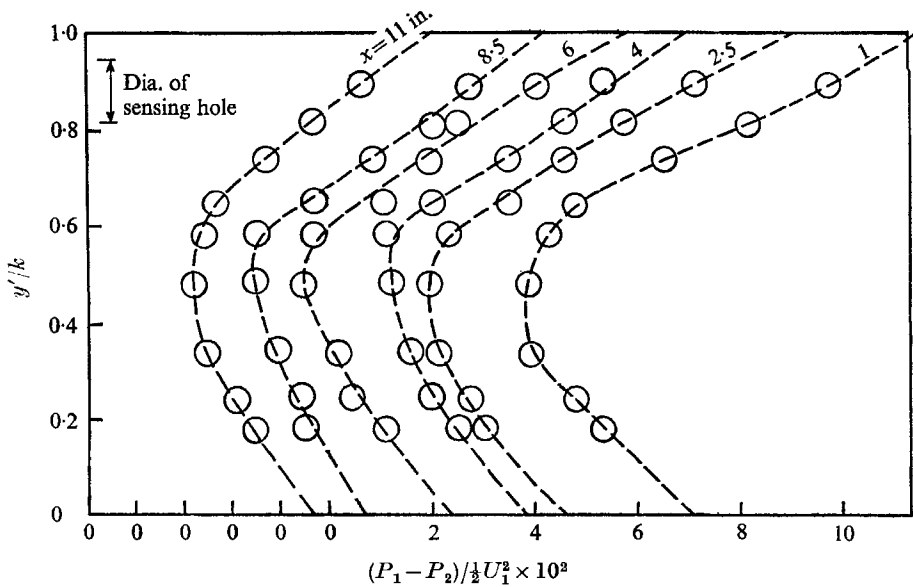


FIGURE 3. Pressure difference profiles in the region near the step. $U_1 \delta_s / \nu \simeq 3.1 \times 10^4$. Note the shift in origin.

Effective wall shear stress values derived from the pressure distributions of figures 3 and 4 through (1), assuming the effective τ_w to be equal to τ_{HG} , are plotted in figure 5. For comparison, skin friction deduced from the 'error in origin' method is also shown (assuming the error in origin $\epsilon = 0.08$ in. or $\epsilon/k = 0.64$ at all stations, a value which seems to give an acceptable, though by no means unique, logarithmic region even at $x = 2$ in., as shown in figure 6), but, as has already been stated, the basis of this method is questionable at least near the start of the roughness. Close to the start of the roughness, the form drag results may also be in error due to the doubt expressed concerning assumptions (ii) and (iii) used in the derivation of equation (1). Generally there may also be an error due to uncertainty in the shape of the pressure distributions near the crest and near the base of the elements, and to the errors involved in measurement of small pressure differences. The wall shear stress, derived from the momentum thickness distribution shown later in figure 8, is, however, in better agreement with

the trend and magnitude of the form drag results than with those obtained from the error in origin method.

All methods used give a distribution of c_f which is in qualitative agreement with

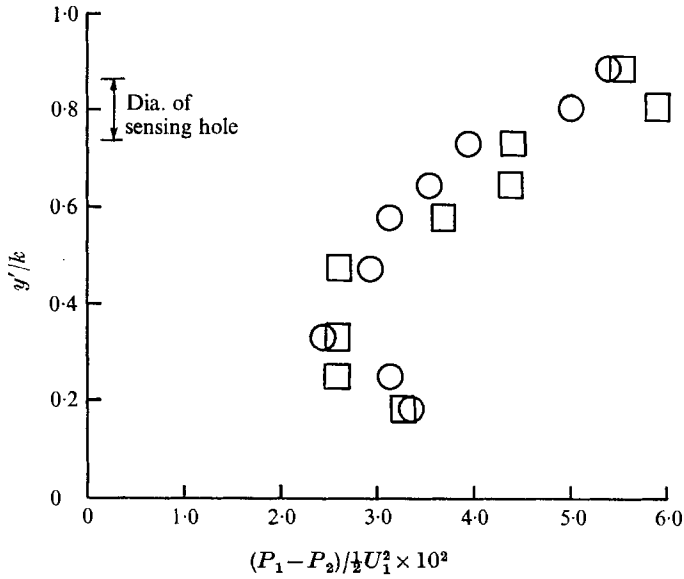


FIGURE 4. Pressure difference profiles at $x = 46.5$ in. from step. \circ , $U_1 \delta_s / \nu \approx 3.1 \times 10^4$; \square , 1.9×10^4 .

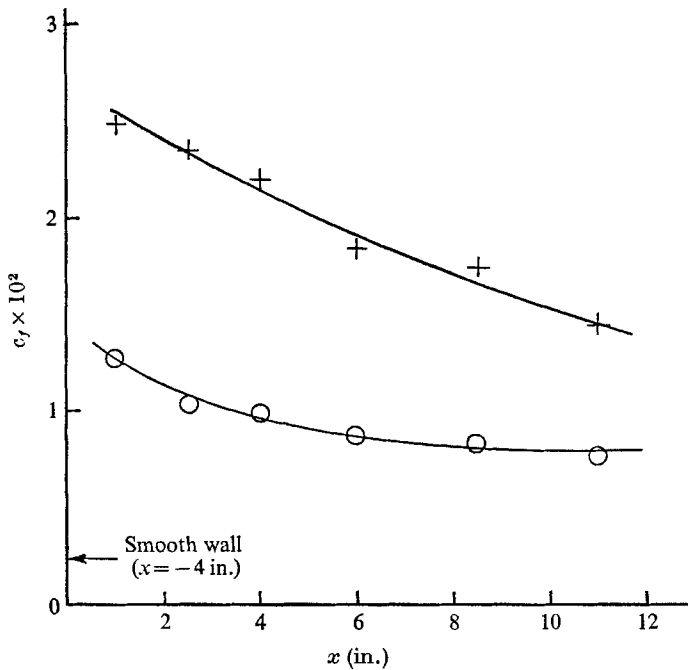


FIGURE 5. Variation of effective wall shear stress near the step. $U_1 \delta_s / \nu \approx 3.1 \times 10^4$. \circ , determined from form drag of roughness elements; +, determined from 'error in origin' method assuming $\epsilon = 0.08$ in. at all stations.

the prediction methods referred to in § 1, even though these methods are probably not strictly applicable to the present case. There is a sudden rise in c_f at the start of the roughness, followed by a fairly rapid fall towards the value applicable to the fully rough layer. Thus, the skin friction appears to adjust rapidly, within 3 or 4 boundary-layer thicknesses, to the new rough wall boundary condition.

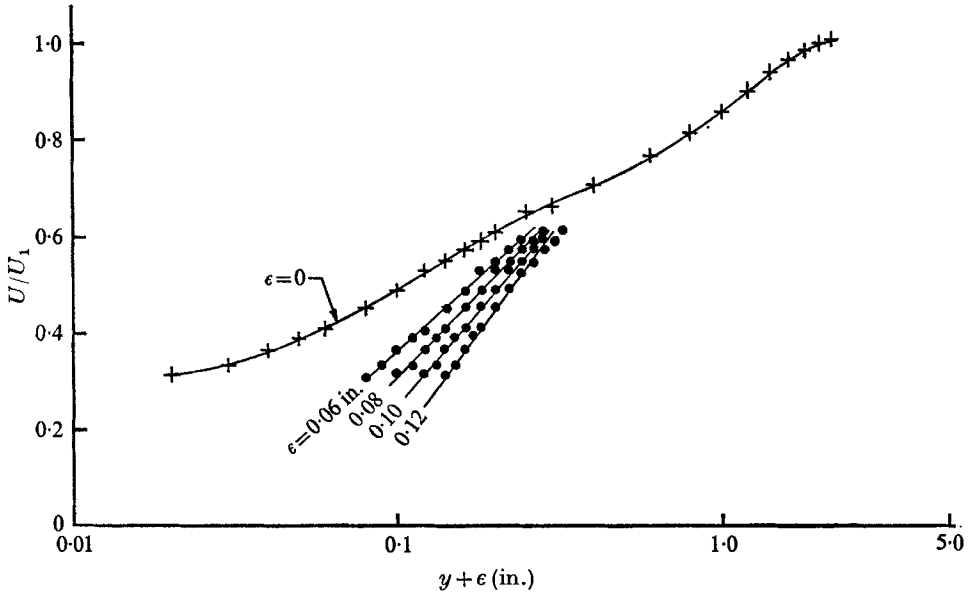


FIGURE 6. Example of 'error in origin' method of obtaining a logarithmic profile at $x = 2$ in. $U_1 \delta_s / \nu \simeq 1.9 \times 10^4$.

4. Self-preservation of mean velocity field

Mean velocity profiles at four stations on the rough wall are plotted in figure 7 in the form $(U_1 - U)/U_\tau$ as a function of $(y + \epsilon)/\Delta$, where $\Delta = \delta^* U_1 / U_\tau$ and ϵ , the error in origin, is assumed to be constant and equal to 0.08 in. The distributions at $x = 35$ in. and $x = 45$ in. fall, within experimental scatter, on the same curve over almost the complete range of $(y + \epsilon)/\Delta$. Since the mean velocity defect at $x = 20$ in. exhibits only a slight departure from this curve for the larger values of $(y + \epsilon)/\Delta$, it is reasonable to assume that self-preservation of the mean flow field is attained by $x = 35$ in. The profile defect parameter,

$$G = \int_0^\infty \left(\frac{U_1 - U}{U_\tau} \right)^2 d \left(\frac{y + \epsilon}{\Delta} \right), \quad (2)$$

is found to be equal to about 6.8 for the mean velocity distribution at $x = 45$ in. Values of G reported in the literature for the universal velocity profile on a smooth or rough wall in a zero pressure gradient usually lie between 6.0 and 7.0.

The shape parameter $H = \delta^*/\theta$, plotted in figure 8, increases from a value of 1.4 on the smooth wall to a value of about 1.8 at $x \simeq 25$ in., and it maintains this value up to $x \simeq 60$ in. At larger values of x a slow decrease in H is observed.

The displacement thickness δ^* and the momentum thickness θ increase almost linearly with x , except very close to the surface change (figure 8). For the range of x over which H is approximately constant, the streamwise variation

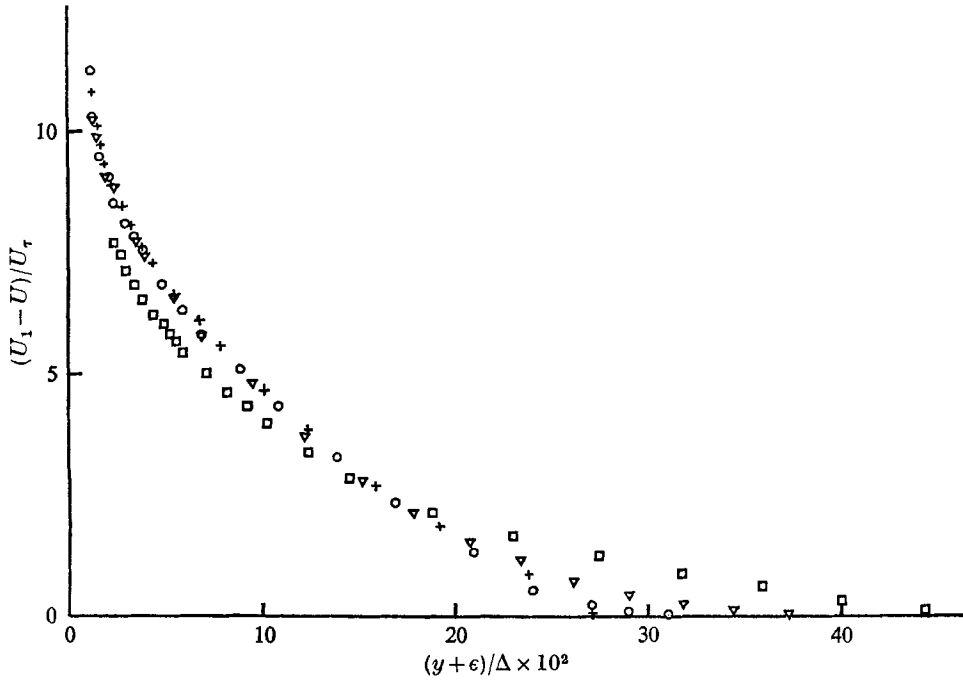


FIGURE 7. Mean velocity defect profiles on the rough wall assuming $\epsilon = 0.08$ in. for each profile. $U_1 \delta_s / \nu \approx 1.9 \times 10^4$. \square , $x = 10$ in.; ∇ , 20; $+$, 35; \circ , 45.

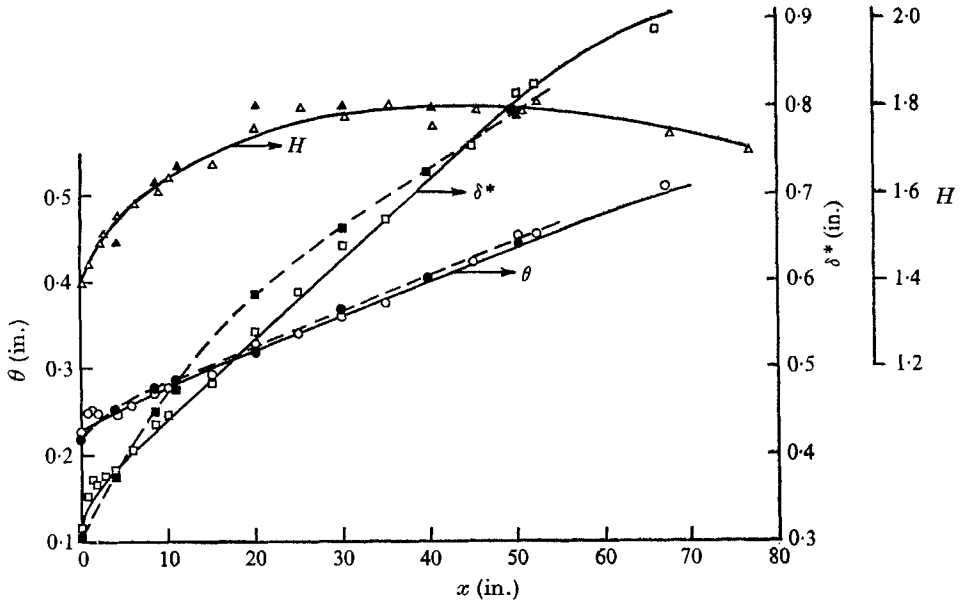


FIGURE 8. Distributions of δ^* (\circ , \bullet); θ (\square , \blacksquare); $H = \delta^*/\theta$ (\triangle , \blacktriangle). \circ , \square , \triangle , —, $U_1 \delta_s / \nu \approx 1.9 \times 10^4$. \bullet , \blacksquare , \blacktriangle , - - -, $U_1 \delta_s / \nu \approx 3.1 \times 10^4$.

of θ implies a constant value of c_f of about 0.0084 for both Reynolds numbers investigated. From the above definition of G , a relation between H and G can be written

$$H = (1 - G(c_f/2)^{\frac{1}{2}})^{-1}. \quad (3)$$

For $c_f = 0.0084$ and $G = 6.8$, H equals 1.79 which is in good agreement with the experimental values of figure 8.

5. Method of plotting mean profiles

In the study of the response of a turbulent boundary layer to an upstanding step-change in surface roughness (Antonia & Luxton 1971 *a*), it was observed that the mean velocity profiles inside the internal layer in the region near the step exhibited a linear trend when plotted in the form U vs. $y^{\frac{1}{2}}$. It was also found that the mean velocity distribution outside the internal layer could conveniently be plotted in the same co-ordinates, exhibiting a different linear trend except very near the outer edge of the layer. The intersection of the two straight lines was shown to be closely related to the edge of the internal layer. A weak dimensional argument was given to support the half-power plotting scheme, but this required that the streamwise gradient of wall shear stress $d\tau_{w2}/dx$ immediately downstream of the step be included in the argument in place of the wall shear stress τ_{w2} . Difficulties in making adequate measurements in that particular flow, occasioned mainly by the presence of a separation bubble with unhappy stability characteristics behind the upstanding first element, and the problem of measuring τ_{w2} , left the dimensional argument with neither direct support nor denial.

In the present experimental configuration, no first element separation bubble was present, and hence quite detailed measurements could be made, though some doubt must remain about the accuracy of the effective wall shear stress. Nevertheless, the variation of c_f shown in figure 5 hardly suggests that $d\tau_{w2}/dx$ is a dominant parameter close to the start of the roughness. The local shear stress gradient $|\partial\tau/\partial y| = \alpha$ is, however, likely to be large in the region near the step, as the magnitude of τ_{w2} is certainly large compared to that of τ_{w1} on the smooth wall immediately upstream of the roughness, and the shear stress in the internal layer must vary between τ_{w2} at the surface and a value of the same order as τ_{w1} near the edge of the internal layer. It is probable, then, that $\partial\tau/\partial y$ has a strong influence on the velocity profile in the internal layer. This profile will also be influenced by the distance from the surface y , the wall stress τ_{w2} and some length scale associated with the roughness height k . Viscosity is not likely to be significant, as the flow is fully turbulent at least down to the crests of the roughness elements. Thus, we write

$$U = U(y, \alpha, \tau_{w2}, k). \quad (4)$$

If it is now assumed that the relative motions inside the internal layer are mainly determined by α , i.e.

$$\partial U/\partial y = \partial U(y, \alpha)/\partial y, \quad (5)$$

dimensional considerations then yield

$$\frac{\partial U}{\partial y} \sim \alpha^{\frac{1}{2}} y^{-\frac{1}{2}}. \quad (5a)$$

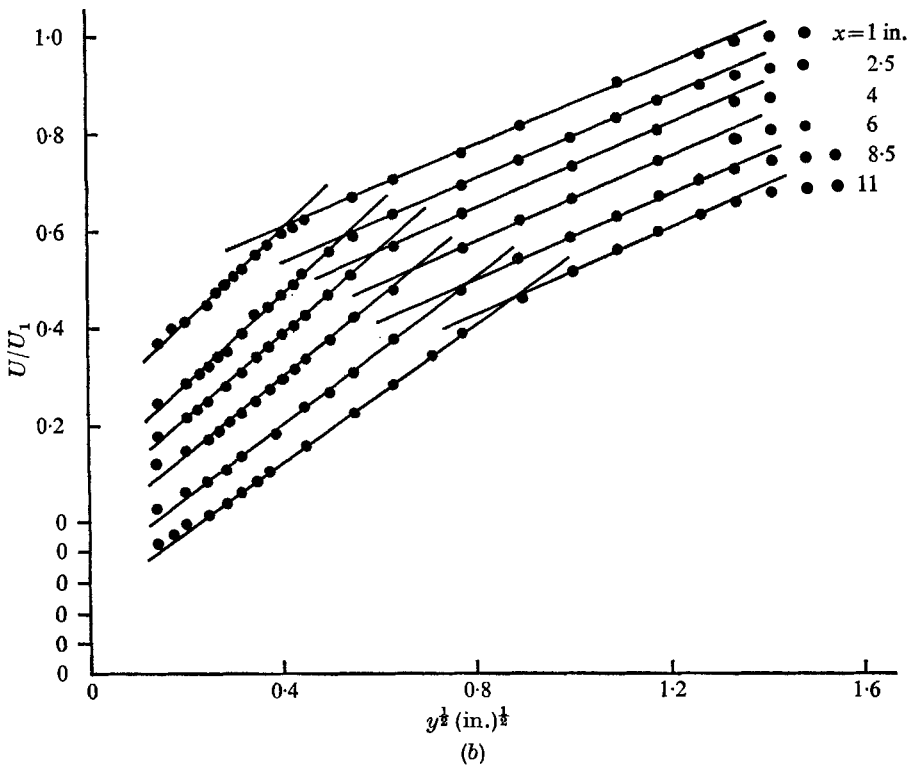
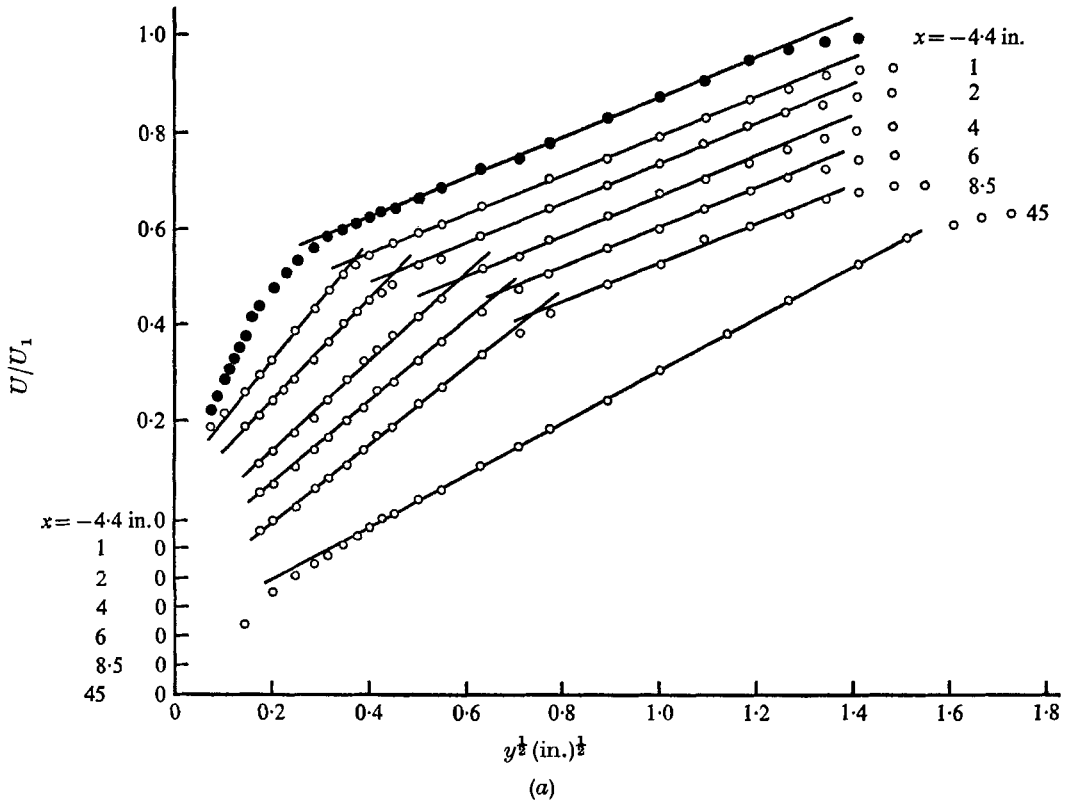


FIGURE 9. Mean velocity profiles plotted as a function of $y^{1/2}$. (a) $U_1 \delta_s / \nu \simeq 1.9 \times 10^4$, (b) $U_1 \delta_s / \nu \simeq 3.1 \times 10^4$. Note shift in origin.

If it is further assumed that α is independent of y , then integration of (5a) results in a half-power velocity profile, with the integration constant being presumably a function of $\alpha k/U_7^2$. Examples of mean profiles plotted in this form are shown in figures 9(a) and (b). This last assumption, that $\alpha = |\partial\tau/\partial y|$ is independent of y , is supported by the distributions of the shear stress $-\overline{uv}$ in the region near the step, presented in figure 12(b) and discussed in §7. For present purposes, it is sufficient to note that, within experimental accuracy, reasonable straight line fits are obtained for the majority of the \overline{uv} profiles in the internal layer. As x increases, there is a tendency for $-\overline{uv}$ to decrease as the wall is approached. From the slopes of the straight lines as shown in figure 12(b), it is seen that $|\partial\tau/\partial y|$ decreases as x increases. From the half-power mean velocity profile plots, figures 9(a) and (b), it is evident that $\partial U/\partial y^{\frac{1}{2}}$ also decreases as x increases lending at least qualitative support for the form of (5a). The main argument in favour of the half-power method of plotting mean profiles must remain, however, the convenience of being able to estimate the position of the edge of the internal layer from the 'knee' in the velocity profile plots.

6. Growth of the internal layer

The approximate position of the edge of the internal layer has been estimated in two ways. As mentioned in §5, it was shown in Antonia & Luxton (1971*a*) that the 'knee' point, the intersection of the straight lines on the half-power plot U vs. $y^{\frac{1}{2}}$, could conveniently be used to define the edge δ_i of the internal layer. The position of the knee point deduced from the half-power plots presented in §5, is shown in figure 10 for various values of x . An adequate fit to the results is given by $\delta_i \propto x^{0.72}$, corresponding to a faster rate of growth of the internal layer than for the case of an upstanding roughness change†.

A physically more realistic determination of δ_i may be obtained by inferring the 'merge' point (or the position of merging) between consecutive mean velocity profiles. The results presented in §2 show that this point also closely coincides with the merging of the turbulence intensity profiles. In the present study, the position of the merge point was inferred by superposing mean velocity profiles (plotted on either a linear or a half-power scale) obtained at successive streamwise stations. The values of δ_i obtained (figure 10) are slightly higher than those determined by the knee point, whilst the rate of growth of δ_i is now represented by $\delta_i \propto x^{0.79}$, which is reminiscent of the growth rate of a turbulent boundary layer developing in a uniform free stream. Here, the effect of a small streamline displacement is included in the determination of δ_i .

The experimental values of δ_i , estimated from the merge point, are compared in figure 11 with the theoretical predictions of Elliott (1958) and of Townsend (1965) in the region near the step. Although the theory of Elliott, and in particular that of Townsend, is not strictly valid for small values of x/z_{02} , it is seen that the experi-

† Note, however, that because of the initial thickening of the internal layer produced by the separation bubble from the first element in the upstanding roughness case, the physical thickness was greater than in the present case even though the growth rate was less.

mental rate of growth of δ_i is in reasonable agreement with the theories; but the experimental values of δ_i/z_{02} are significantly smaller than the predicted values.

To compute these values, a constant value of the equivalent roughness length scale z_{02} was assumed on the rough wall. This value is obtained by extrapolating

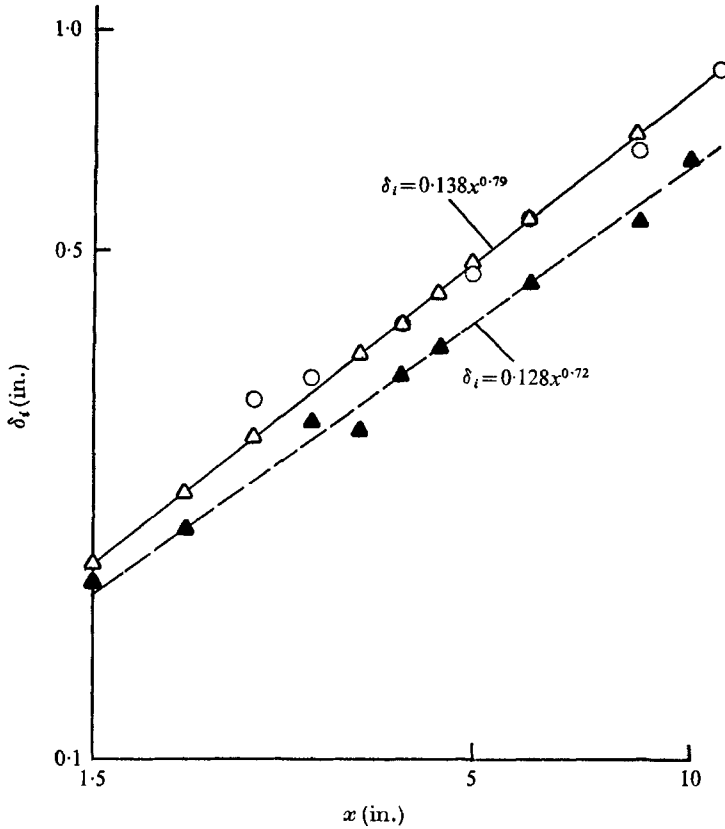


FIGURE 10. Growth-rate estimates for the internal layer. \circ, Δ , estimates from profile 'merge' points. \blacktriangle , estimates from the 'knee' points. $\circ, \Delta, U_1 \delta_i / \nu \simeq 3.1 \times 10^4$; $\Delta, \blacktriangle, 1.9 \times 10^4$.

the (assumed) logarithmic distribution to zero velocity. The assumed distribution for a fully rough wall layer is

$$\frac{U}{U_\tau} = \frac{1}{\kappa} \ln \frac{y'' U_\tau}{\nu} + A - \frac{\Delta U}{U_\tau}, \tag{6}$$

where κ is the Kármán constant, y'' is the effective distance from the wall, A is a constant taken here to be 4.9, and $\Delta U/U_\tau$ is the roughness function (Clauser 1956) given by

$$\frac{\Delta U}{U_\tau} = \frac{1}{\kappa} \ln \frac{k U_\tau}{\nu} + D. \tag{7}$$

For the present experiments, the best fit line gives $D = 1.8$. Using these expressions we obtain

$$z_{02} = k \exp[\kappa(D - A)], \tag{8}$$

which gives, for the stated values of A and D , $z_{02} = k/3.56$. The roughness step M is defined by $M = \ln z_{02}/z_{01}$, where z_{01} is the equivalent roughness length scale on the smooth wall; and, for the present case, M is about -4.6 .

In considering the above comparison, we must anticipate a conclusion drawn in §8, that the assumption $L_e = \kappa y$ breaks down in the inner layer similarity is not applicable. As both the theoretical methods require such similarity, it is not surprising that the predictions are poor for the present case.

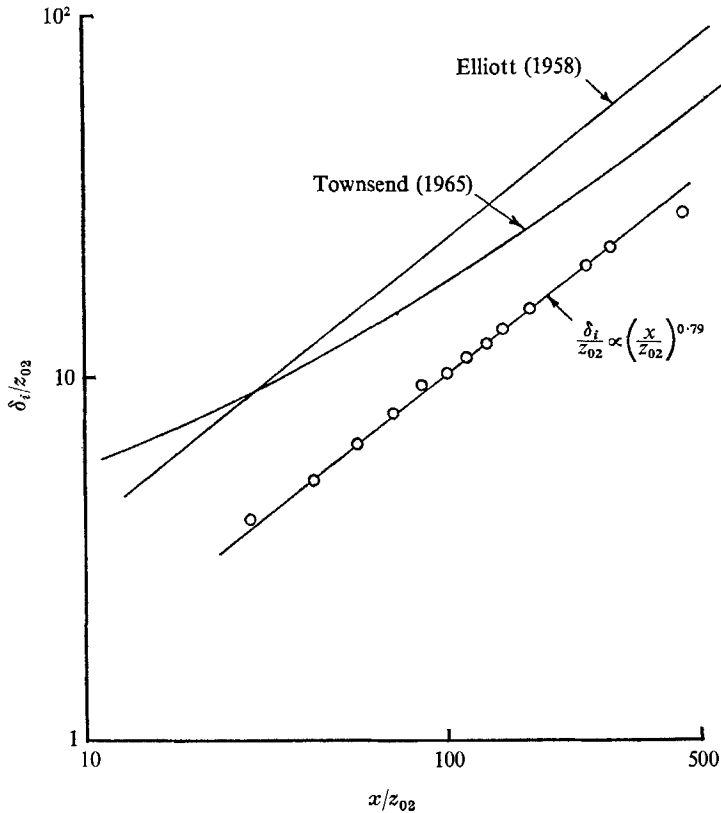


FIGURE 11. Comparison of experimental growth of internal layer with theories of Townsend (1965) and Elliott (1958). $U_1 \delta_s / \nu \simeq 1.9 \times 10^4$, $z_{02} \simeq k/3.56$, $M = \ln z_{01}/z_{02} \simeq -4.6$.

7. Discussion of turbulent intensity data

Figure 12(a) shows distributions of $\sqrt{u^2}/U_1$ and $\sqrt{v^2}/U_1$, the normalized root-mean-square values of the turbulence intensities in the longitudinal and vertical directions respectively. Figure 12(b) shows the distribution of $-2\overline{uv}/U_1^2$, the normalized Reynolds shear stress, immediately downstream of the roughness step at the Reynolds number of $U_1 \delta_s / \nu \simeq 1.9 \times 10^4$. As all the quantities shown in figure 12 were obtained with an X -probe, measurements very near the wall were not possible. For this reason, a single wire was used to obtain the shapes of the u -component distributions in the region near the wall. These distributions,

which are plotted on a semi-log basis in figure 13, are in reasonable agreement with those of figure 12 (*a*) for y greater than 0.1 in. They show that near the wall (y less than 0.1 in.), \bar{u}^2 is first increased relative to its smooth wall distribution ($x = -4$ in.) in accord with the sudden increase in the average velocity gradient $\partial U/\partial y$ and the accompanying increase in the turbulent energy production $\tau \partial U/\partial y$. As x increases, however, $\partial U/\partial y$ and $\tau \partial U/\partial y$ both decrease in this region (this appears to be consistent with the decreasing trend of the skin-friction results, shown in figure 5), and \bar{u}^2 is correspondingly reduced. Away from the wall (y greater than 0.1 in.), \bar{u}^2 increases with x in accord with the streamwise increase in $\partial U/\partial y$ over the outer part of the internal layer, and the internal layer extends progressively further into the outer region of the original smooth wall boundary layer.

The distributions of \bar{v}^2 and $-\bar{w}^2$ show the same trend† as that of the \bar{u}^2 profiles. It is observed that, within the experimental accuracy, all of the turbulence intensity profiles over the initial part of the rough wall merge into the corresponding distributions on the smooth wall at values of y which are in close agreement with the edge of the internal layer as inferred from the 'merge' point of the mean velocity profiles (see §6). In figure 12 (*b*) the $-\bar{w}^2$ distribution on the smooth wall ($x = -4.4$ in.), which was obtained with a DISA X -probe, extrapolates to a wall value which corresponds to a skin-friction coefficient of about 0.0026. This value is significantly lower than the Clauser chart value of 0.0034‡ deduced from a mean velocity profile at this station. As a check, a complete set of $-\bar{w}^2$ distributions were obtained with a rotating wire. At $x = -2.5$ in., a wall value of about 0.0032 is suggested from three measurements in better agreement with the Clauser chart value. The shape of the smooth wall \bar{w}^2 distribution obtained with the X -wire is compatible with a constant shear stress in the region near the wall, but its magnitude in this region is lower than that obtained with the rotating probe§. In the outer part of the smooth wall boundary layer, the two distributions are in

† This trend is in agreement with that indicated by the turbulence measurements downstream of an upstanding roughness change (Antonia & Luxton 1971*a*).

‡ It should be noted that independent checks of this value were obtained with a Preston tube, and by application of the momentum integral method.

§ It was found that, although \bar{u}^2 and \bar{v}^2 distributions on the smooth wall agreed well with those obtained in self-preserving smooth wall boundary layers by other workers, the \bar{w}^2 distribution was generally lower than expected. Careful testing of a range of probe designs, including commercial probes, indicated that in all but one case the measured value of \bar{w}^2 was low at the Reynolds number of the tests reported in this paper. The shapes of the distributions were not distorted. At higher Reynolds numbers, the distributions all agreed with those of Klebanoff (1955). The probe that gave the 'correct' distribution at the lower Reynolds number (i.e. a distribution which extrapolated to the wall shear value as determined from a Clauser chart) was of the single inclined rotating-wire type, and this probe was also 'correct' at the higher Reynolds number. It was concluded that the low values of \bar{w}^2 at the lower Reynolds number did not indicate a lack of full boundary-layer development, but did indicate that X -wire configurations may be Reynolds number dependent at low Reynolds numbers. The results presented here are those obtained with an X -wire configuration, and were all obtained at the lower Reynolds number. Accordingly, the \bar{w}^2 distributions lie below those of Klebanoff, but, as the shapes of the distributions are not affected, and the results are internally consistent, the conclusions drawn from them are not seriously in question.

reasonable agreement with each other. Over the roughness, the magnitude of the X-wire distribution of $-\overline{wv}$ in the internal layer is lower than that of the rotating wire distribution at the same station, but, apart from the scatter in the experimental points, these distributions are similar in shape. The fact that the shapes of

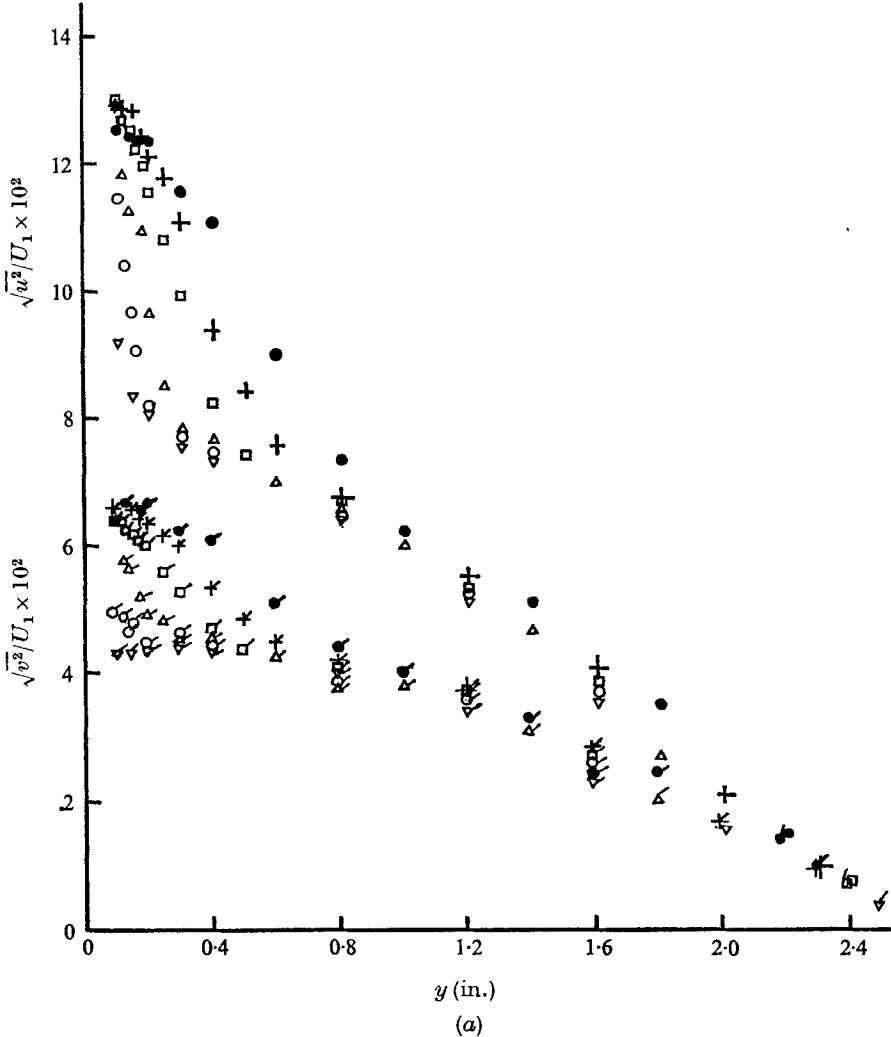


FIGURE 12(a). For legend see facing page.

the distributions are similar will be seen to be particularly important in discussion of the $-\overline{wv}$ distributions near the rough wall. It is difficult to reconcile the absolute values of \overline{wv} in the region near the wall with the skin-friction results presented in §3. The straight-line approximations to the \overline{wv} distributions obtained with the rotating wire extrapolate to wall values which are smaller than those deduced from the form drag measurements, but there does not appear to be any irrefutable physical reason to expect such an extrapolation to reach the effective wall shear stress value.

The shear stress distributions at $x = 6$ in. and $x = 10$ in. (figure 12(b)) show that $-\overline{uv}$ tends to decrease as the wall is approached. This trend becomes more pronounced at larger values of x (figure 14(b)). Figures 14 show the distributions

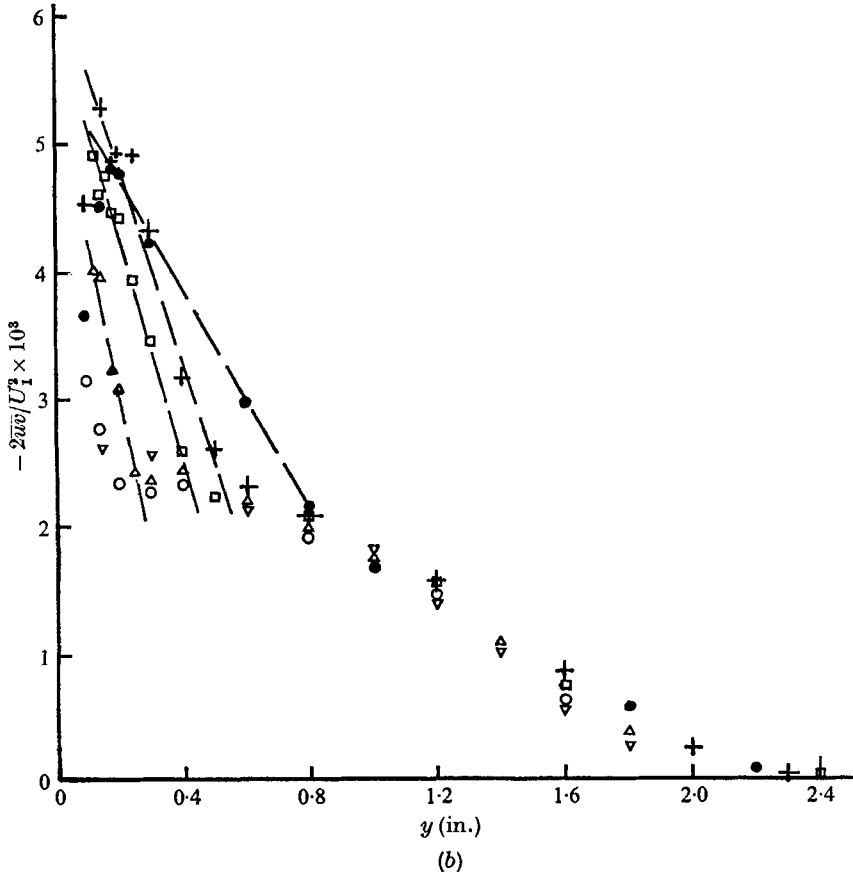


FIGURE 12. Turbulence intensities and shear stress at stations near to the step change in roughness, $U_1 \delta_s/\nu \simeq 1.9 \times 10^4$. (a) u - and v -component intensities. Unflagged symbols refer to $\sqrt{u^2}/U_1$ and flagged symbols to $\sqrt{v^2}/U_1$. (b) Shear stress $-2\overline{uv}/U_1^2$ obtained with an X-wire. The straight-line fits to distributions near the wall support the half-power data correlation scheme for mean velocity profiles.

▽	○	△	□	+	●
$x = -4.4$ in.	1	2	4	6	10

of $\sqrt{u^2}/U_1$, $\sqrt{v^2}/U_1$ and $-2\overline{uv}/U_1^2$ plotted against y/δ^* , where δ^* is the displacement thickness of the boundary layer for larger values of x . At $x = 35$ in., the distributions of u^2 and v^2 become approximately similar in shape over a large fraction of the boundary-layer thickness tending to suggest that the self-preservation of the normal stresses is attained reasonably rapidly. The distributions of u^2 and v^2 on the smooth wall are also plotted in figure 14(a) for comparison with those on the rough wall. From figures 13 and 14(a), after rescaling with δ , it may be seen that the magnitudes of u^2 and v^2 in the outer part of the rough wall boundary layer are significantly higher than those on the smooth wall. It is reasonable to infer that

the integrated turbulent energy $\frac{1}{2} \int \overline{q^2} dy$ where $\overline{q^2} = \overline{u^2} + \overline{v^2} + \overline{w^2}$, is higher on the rough wall, and, as a large proportion of this energy occurs well away from the wall, one might anticipate that it is associated with the larger length scales. Near the roughness, and well downstream of the change, $\overline{u^2}$ and $\overline{v^2}$ increase with distance from the wall, the increase in $\overline{v^2}$ being slower; but over most of the inner layer ($y/\delta \leq 0.15$), $\overline{u^2}$ and $\overline{v^2}$ may be assumed to remain approximately constant.

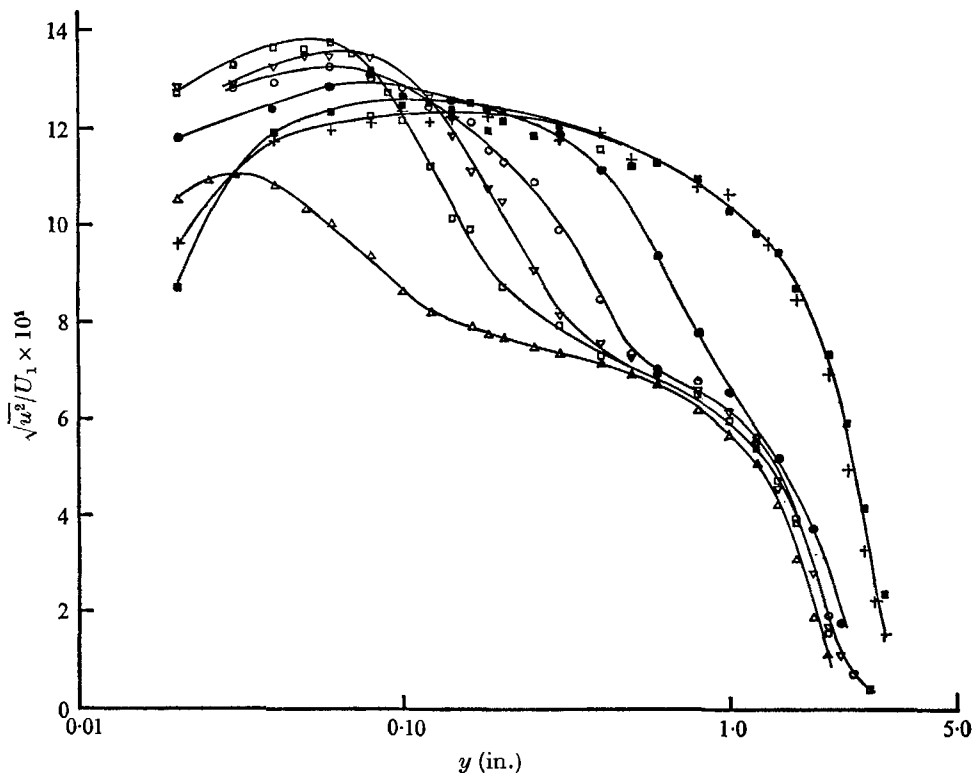


FIGURE 13. Streamwise component of turbulence intensity obtained with a single wire, $U_1 \delta_s/\nu \simeq 1.9 \times 10^4$. Δ , $x = -4$ in.; \square , 1; ∇ , 2; \circ , 4; \bullet , 10; $+$, 45; \blacksquare , 52.

The shapes of the $-\overline{uv}$ distributions in the outer part of the rough wall boundary layer also appear to be reasonably similar, tending to confirm the above claim of approximate self-preservation. In the region corresponding to the inner layer, the shear stress decreases as the wall is approached. At $x = 46.5$ in., for example, the decrease starts from $y/\delta \simeq 0.25$, where $-2\overline{uv}/U_1^2 \simeq 0.0052$, this value being considerably lower than the skin-friction coefficient value of 0.0084 obtained by applying the momentum-integral method at this station. A similar trend of $-\overline{uv}$ near the wall is also evident in the limited experimental data of Chanda (1958) and Makita (1968). Chanda reports two distributions of \overline{uv} measured at the same station on a rough surface, which consisted of crushed stone ranging from 0.25 in. to 0.315 in. in size. The boundary-layer thickness was about 6.5 in. These distributions exhibit a peak at $y/\delta \simeq 0.25$, the value of $-2\overline{uv}/U_1^2$ at this peak being

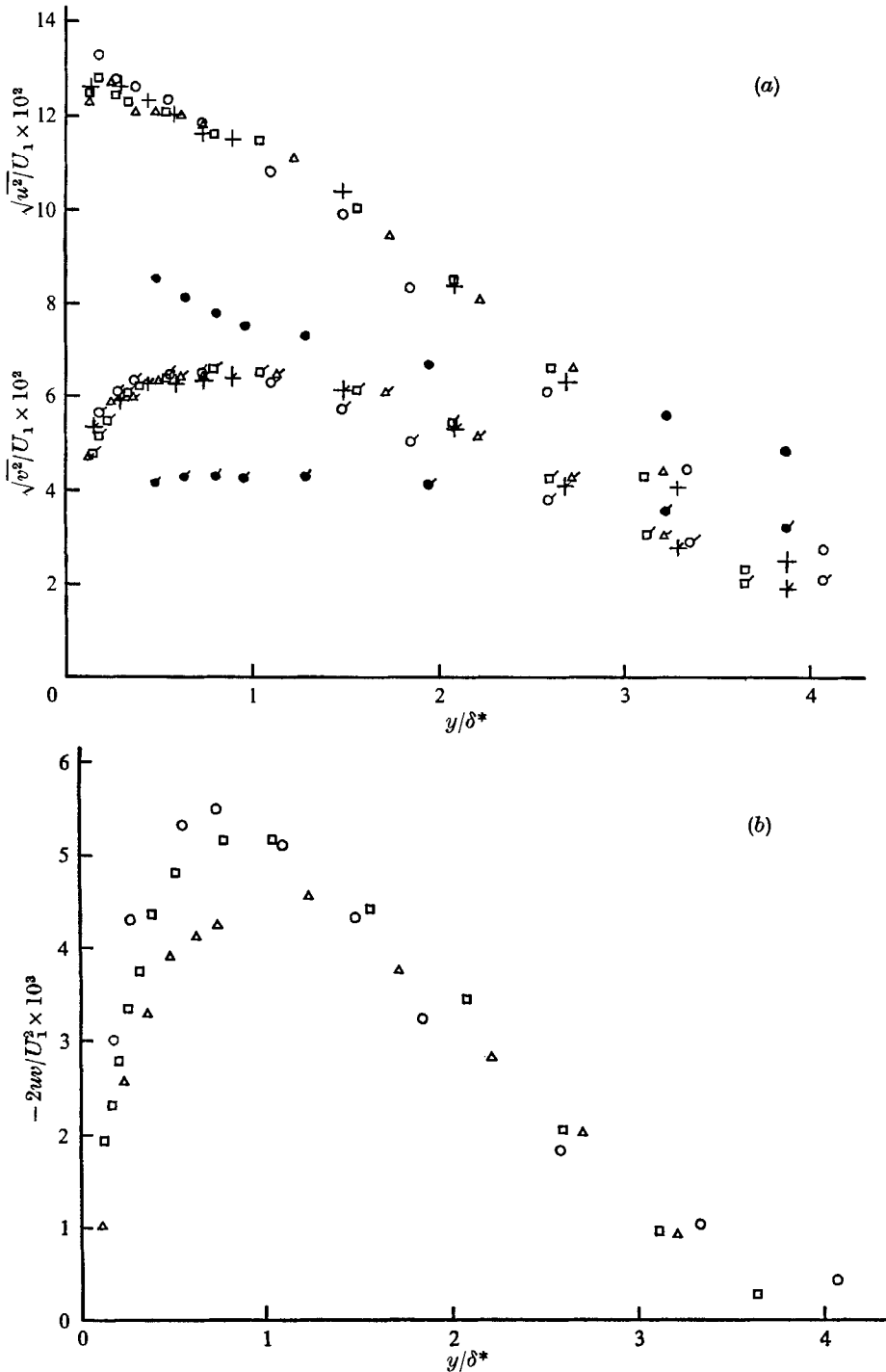


FIGURE 14. Turbulence intensities and shear stress at stations well downstream from the step change in roughness, $U_1 \delta_s / \nu \simeq 1.9 \times 10^4$. (a) u - and v -component intensities. Unflagged symbols refer to $\sqrt{u^2}/U_1$ and flagged symbols to $\sqrt{v^2}/U_1$. Smooth wall results are included for comparison. (b) Shear stress $-2\overline{uw}/U_1^2$ obtained with an X -wire. Values of c_f obtained from the momentum integral equation are $x = 20$ in., $c_f = 0.0086$; 46.5 , 0.0084 ; 50 , 0.0084 .

●	$x = -4.4$ in.,	$\delta^* = 0.31$,	$\delta = 1.9$
○	20	0.54	2.4
+	35	0.67	2.7
□	46.5	0.77	2.9
△	50	0.81	3.0

approximately 27% lower than the value of c_f given by $2d\theta/dx$. Makita's investigation was mainly concerned with the experimental study of the flow field downstream of a rough-to-smooth step change in surface roughness in a two-dimensional channel. The roughness geometry used was somewhat similar to that being studied here except that the ratio λ/k was equal to about 6.7. The distribution of $-\overline{uv}$ on the roughness element just ahead of the smooth surface reveals a peak at $y/d \simeq 0.20$ (d is the half-height of the channel), the value of $-2\overline{uv}/U_1^2$ at this peak being approximately 40% lower than the wall value obtained from the static pressure drop.

Chanda tentatively suggested that this apparent discrepancy in his results may be due to the neglect of the normal stress terms in the momentum integral equation,

$$c_f = 2 \frac{d\theta}{dx} - 2 \frac{d}{dx} \int_0^\delta \frac{\overline{u^2} - \overline{v^2}}{U_1^2} dy. \quad (9)$$

At $x = 46.5$ in. in the present experiments, the contribution due to the second term on the right-hand side of equation (9) represents only about 5% of the magnitude of $2d\theta/dx$. Chanda has also stated that the total resistance in the layer near the rough surface is due to the drag on the roughness, as well as to the Reynolds shear stress, and therefore the measured values of \overline{uv} will not give the total shear stress near the surface. It is likely that the periodic nature of the present rough wall causes the mean streamlines near the roughness crest to be wavy, and a term such as $\langle UV \rangle / U_1^2$ (see §3) may be significant. The possibility that the distortion of the mean streamlines in the vicinity of the roughness elements may affect the measurements of \overline{uv} cannot, however, be entirely discarded. For the present investigation, it was assumed that the mean velocity vector near the wall was parallel to the base of the rough surface. The mean velocity profiles obtained with a single wire showed that the mean value of V (as obtained with the equation of continuity) was small compared with the local value of U . The actual variation of V over a distance of one roughness pitch could not be extracted from these results as the single wire responds to the total velocity vector. Also, an X -wire was found to be unreliable for the determination of V . It should also be noted that several \overline{uv} profiles, taken at intermediate positions between two consecutive roughness elements, reveal no significant departure from the shape of the profiles observed above the crest of the roughness.

Another indirect way of determining the shear stress distribution through a boundary layer is by integration of the momentum equation. This method has been used in a rough wall zero-pressure-gradient boundary layer by various workers. The calculated shear stress distributions have in general been similar to those obtained on the smooth wall, with the trend in the vicinity of the wall consistent with the assumption of a constant shear stress (see e.g. Liu *et al.* 1966; Doenecke 1964).

It has been found that the mean velocity profile in the outer part of a rough wall boundary layer follows the same similarity law as that for the outer region of a smooth wall layer. Here we try to ascertain whether the same similarity form also exists for the turbulence intensities measured on the smooth and rough walls. The u - and v -component turbulence intensity profiles at $x = 46.5$ in. are replotted

in figures 15(a) and (b), together with data taken from various sources, in the form $\sqrt{\overline{u^2}}/U_\tau$ vs. y/Δ and $\sqrt{\overline{v^2}}/U_\tau$ vs. y/Δ . Because of the uncertainty in the determination of error in origin ϵ , the value of y has been left uncorrected for the data presented in figures 15†. The addition of ϵ to y should not greatly affect the shapes of the curves, particularly at the larger values of y . It should be noted that the distributions of $\overline{u^2}$ and $\overline{v^2}$ at $x = 46.5$ in. may be regarded as being representative of the majority of the profiles of figure 14(a) for the larger values of x , where the variation of the skin-friction coefficient is small. The data reported by Moore (1951), Corrsin & Kistler (1954) and Liu *et al.* (1966), were obtained at one station only in the flow, and therefore no definite statement can be made about the self-preserving nature of these distributions. In particular, the two profiles of Liu *et al.* (figure 15(a)), which correspond to two different Reynolds numbers, tend to indicate a lack of self-preservation, at least for the lower Reynolds number. Moore's distribution of $\sqrt{\overline{u^2}}/U_\tau$, although somewhat similar in shape to that for the present rough wall data, lies significantly above the other data. The present distribution on the rough wall is in reasonable agreement with that on the smooth wall, except perhaps near the surface where the trend of the smooth wall data is towards the higher values of $\sqrt{\overline{u^2}}/U_\tau$. The distribution of Corrsin & Kistler appears to be high for y/Δ less than about 0.15, but is in reasonable agreement with the present data in the outer region of the boundary layer. Figure 15(b) shows that the present distribution of $\sqrt{\overline{v^2}}/U_\tau$ on the rough wall follows the shape of the smooth wall distribution fairly closely, but its magnitude is slightly low. Also, the decrease in $\sqrt{\overline{v^2}}/U_\tau$ in the wall region is more pronounced in the rough wall boundary layer. Bearing in mind the uncertainty in the origin for y , and the inaccuracy in the determination of c_f ,‡ the assertion that the distributions of $\overline{u^2}$ and $\overline{v^2}$ assume the same similarity shape in the outer part of smooth and rough wall boundary layers is not disproved by the data. The same can probably be said about the shear stress profiles, although the results of figure 16 are even less conclusive, and considerably more evidence is required. The present values of $-\overline{uv}$ are slightly lower in the outer part of the rough wall boundary layer than those on the smooth wall, but the trends followed are reasonably similar. The shear stress values of Corrsin & Kistler appear to decrease near the wall, but their magnitude is significantly higher than the wall shear stress value obtained from the momentum integral equation.

In order to get some idea of the distribution of the turbulence intensities in the region very close to the rough wall, a few measurements were made inside the cavities between roughness elements. These measurements showed that both the mean velocity and the u -component turbulence intensity rise fairly sharply as the top of the cavity is neared. The mean velocity gradient and the gradient of $\overline{u^2}$ are large near the crest of the roughness, and $\overline{u^2}$ reaches a maximum value

† The data reported in Corrsin & Kistler (1954) included a correction for an error in the origin, the ' $y = 0$ ' reference being chosen by extrapolation of the mean velocity profiles in the region outside the corrugation peaks to zero.

‡ The values of c_f indicated in figures 21 and 22 were obtained from the momentum-integral method. One exception is the value of c_f for the results of Liu *et al.* (1966) at $U_1\delta/\nu \simeq 1.8 \times 10^4$, which was inferred from the slope of the logarithmic mean velocity profile.

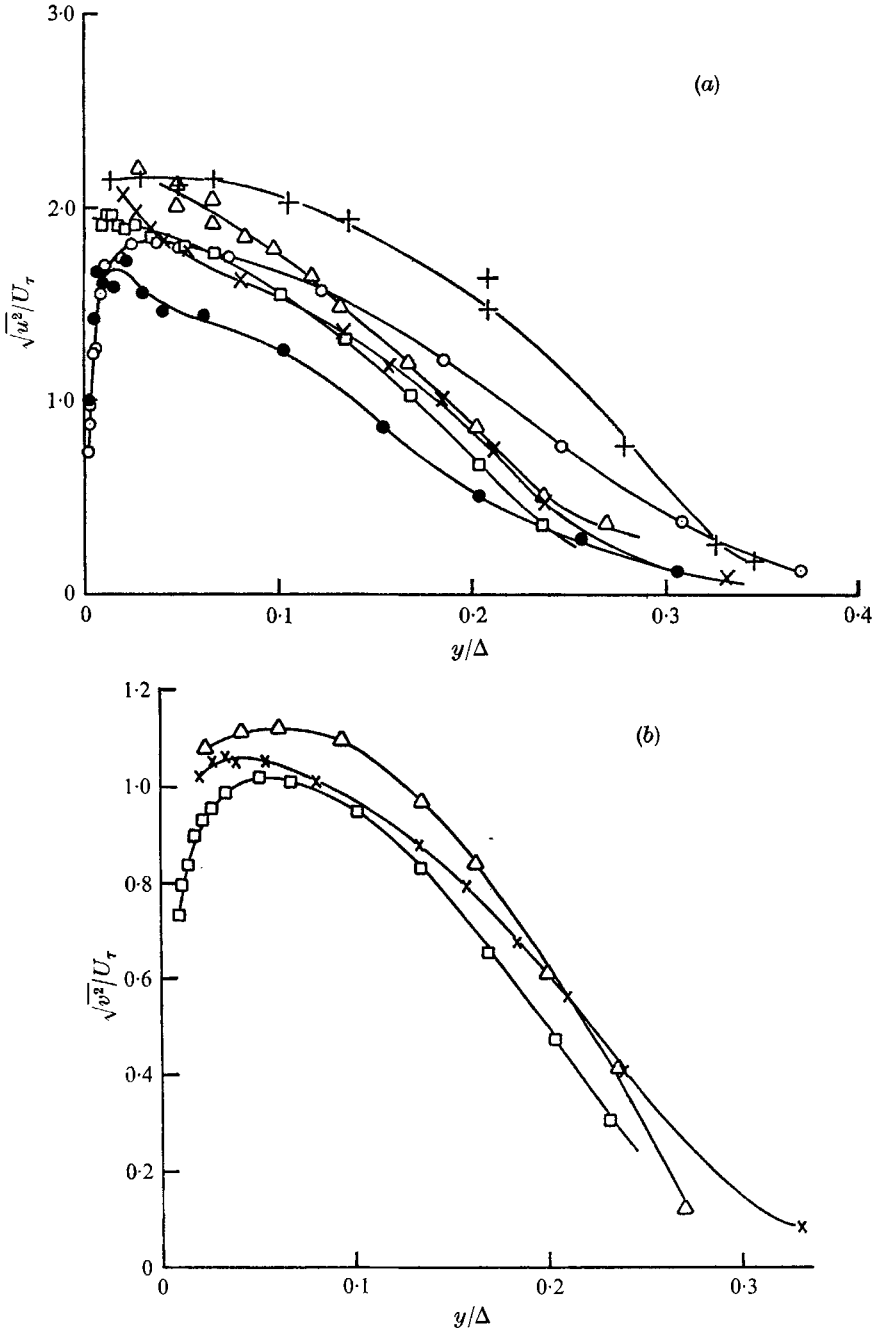


FIGURE 15. Comparison of the distributions of turbulence velocity components on smooth and rough walls. (a) u component, (b) v component.

□	Present data (at $x = 46.5$ in.)	$U_1 \delta / \nu = 2.7 \times 10^4$	$\delta^* / \delta = 0.275$	$c_f = 0.0084$	} Square section roughness $\lambda/k = 4$
+	Moore (1951)	7.8×10^4	0.232	0.010	
○	Liu <i>et al.</i> (1966)	1.8×10^4	0.264	0.0106	
●	Liu <i>et al.</i> (1966)	1.0×10^4	0.262	0.0009	
△	Corrsin & Kistler (1954)	6.5×10^4	0.204	0.0048	
×	Present data	1.9×10^4	0.172	0.0034	Corrugated roughness Smooth wall

a short distance outside the cavity. The distribution of the Reynolds shear stress was measured with a specially designed X-wire, and, while the numerical values obtained must be regarded with suspicion, the shape of the distribution is probably correct. This distribution appears to have a maximum just outside the top of the cavity (at roughly the position at which the maximum of $\overline{u^2}$, occurs), but a second (and more convincingly defined) peak occurs at about 10% of the boundary-layer thickness. As mentioned earlier in §2, this latter peak is observed for all downstream values of x . It is interesting to note that measurements made between elements at $x = 10.75$ in. showed that the maximum value

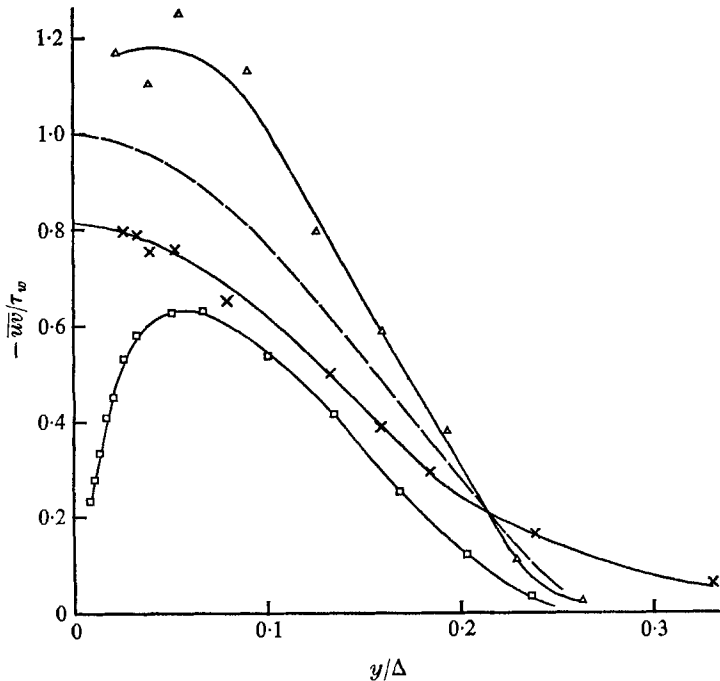


FIGURE 16. Comparison of the distributions of turbulent shear stress on smooth and rough walls. Symbols and data are as for figure 15. ---, the smooth wall distribution of Klebanoff (1955) for $U_1\delta/\nu = 7.5 \times 10^4$ and $c_f = 0.0028$.

of $-\overline{uv}\partial U/\partial y$, the turbulent energy production, occurs immediately above the cavity where the mean velocity gradient is largest. As x increases, however, the peak of $-\overline{uv}$, which appears at the larger value of y , gives rise to a second and much smaller peak in the distribution of $-\overline{uv}\partial U/\partial y$ (see Antonia & Luxton 1971*b*). The distributions of $\overline{u^2}$ and $-\overline{uv}$ in the outer part of the cavity are in qualitative agreement with those obtained by Tani, Iuchi & Komoda (1961) and Haugen & Dhanak (1966) in the free shear layer associated with a single two-dimensional cavity under a thin oncoming turbulent boundary layer.

8. The mixing length and eddy viscosity distributions

The distribution of mixing length $l (= \tau^{1/2} / \partial U / \partial y)$ is shown in figure 17 for various values of x . On the smooth wall ($x = -4.4$ in. and $x = -4$ in.) the values of l obtained in the wall region lie fairly close to the straight line $l = 0.41y$, as expected from local similarity requirements. In the outer region of the boundary layer, l is approximately constant and equal to about 0.08δ , in agreement with the value reported by Bradshaw (1967*a*). Very near the edge of the boundary layer, it is expected that l will increase fairly sharply because $\partial U / \partial y$ decreases

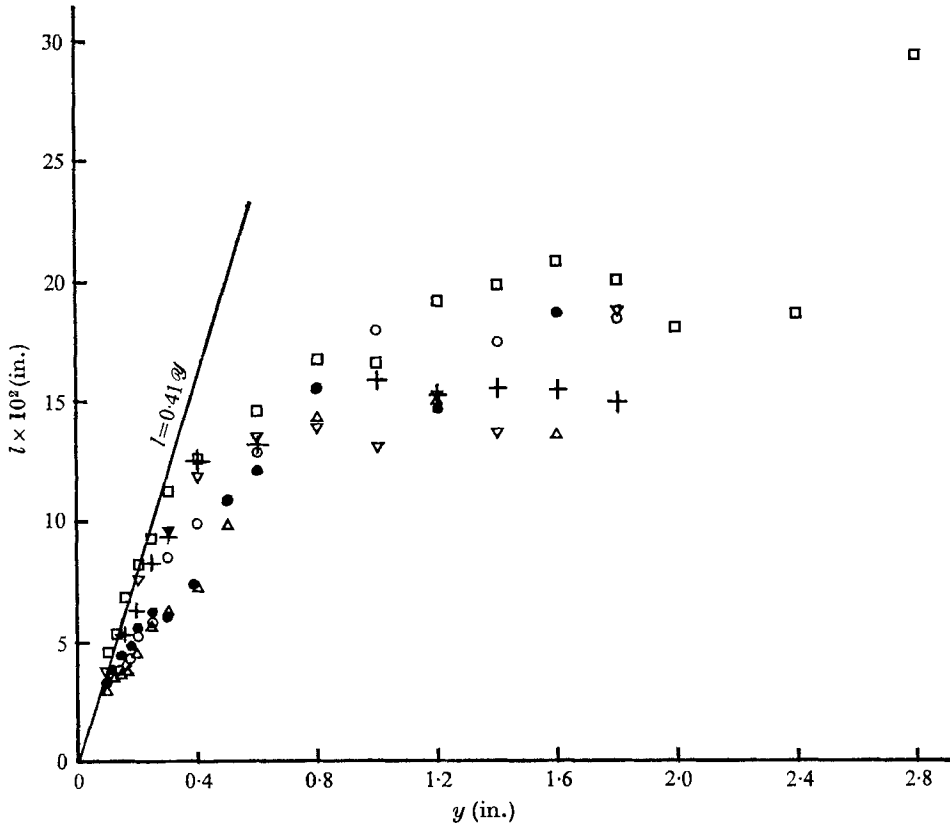


FIGURE 17. Mixing-length distributions. $U_1 \delta_s / \nu \simeq 3.1 \times 10^4$: ∇ , $x = -4$ in.
 $U_1 \delta_s / \nu \simeq 1.9 \times 10^4$: +, $x = -4.4$ in.; \circ , 2; \triangle , 4; \bullet , 6; \square , 46.5.

much more rapidly than τ in this region. As the surface roughness changes, $\partial U / \partial y$ increases near the wall, and, although the shear stress τ is also increased, l appears to be significantly reduced relative to $l = 0.41y$. In the outer part of the boundary layer, where τ and $\partial U / \partial y$ essentially retain their smooth wall values, l should remain unaffected. The scatter in the experimental results in this region is partly due to the small changes in the boundary-layer thickness, and also partly due to errors in the reduction of the data. At $x = 46.5$ in., it is found that the values of l near the wall again follow the line $l = 0.41y$ quite closely, whilst in the outer region l is approximately constant and equal to about 0.07δ .

The distribution of eddy viscosity $\nu_T (= \tau/\partial U/\partial y)$ may be deduced from figures 17 and 14(b). It shows that, in the region very near the wall at small distances downstream from the step, no significant reduction of ν_T relative to its distribution on the smooth wall can be detected. This tends to suggest that, at least in this region, the change in the shear stress τ is closely allied with that in the mean velocity gradient $\partial U/\partial y$. The observed reduction in the mixing length l would be explained by the dependence of l on $\tau^{1/2}$.

The distributions of the ratio $a_1 (= -\overline{uv}/\overline{q^2})$, where $\overline{q^2}$ is assumed to be equal to $(\frac{3}{2})(\overline{u^2} + \overline{v^2})$, are shown in figure 18 for the region near the step. The main feature of these results is that very little change from the distribution of a_1 on the smooth wall can be detected in the region near the wall for small values of x .

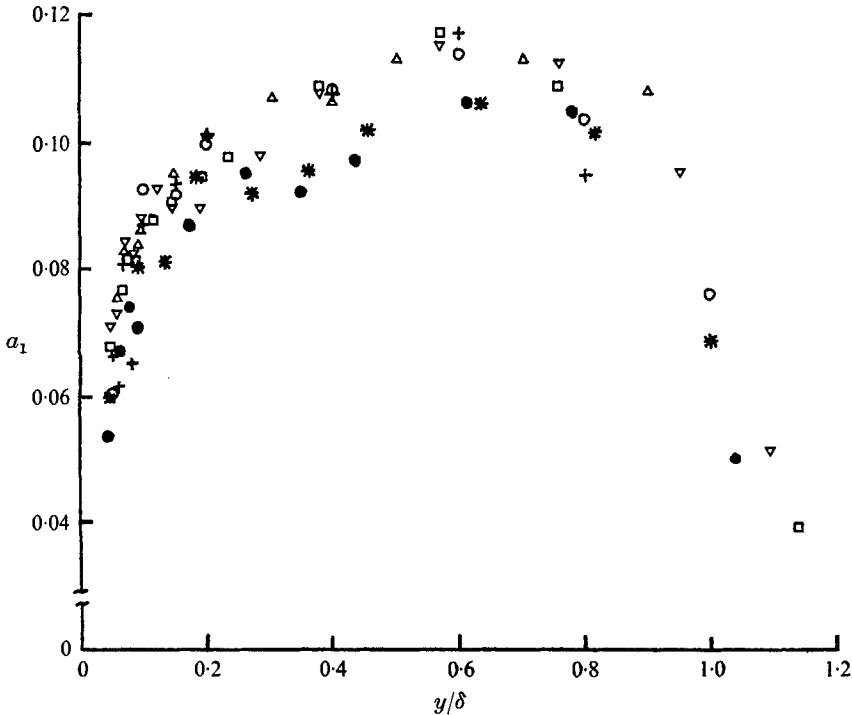


FIGURE 18. Distribution of $a_1 = -\overline{uv}/\overline{q^2}$ in region near the step change, $U_1\delta_s/\nu \approx 1.9 \times 10^4$.

	○	+	△	□	▽	*	●
$x = -2.5$ in.	1	2	4	6	10	15	
$\delta = 1.9$ in.	2.0	2.0	2.1	2.1	2.2	2.3	

The implication is that a close relationship appears to be maintained between τ and $\overline{q^2}$, even though the flow near the wall has been strongly perturbed, and, as will be seen, is far from equilibrium. A comparison of the distribution of a_1 on the smooth wall with that in the self-preserving rough wall boundary layer well downstream shows that a_1 is nearly constant and equal in both layers over a large fraction of the outer layer, with a value of 0.12, which is smaller than the value of 0.14 deduced by Bradshaw (1967a) from the measurements of Klebanoff (1955). In the inner region of the boundary layer, the values of a_1 on the rough wall fall progressively below those on the smooth wall as the wall is approached. It is

possible that this reduction is due to the reported decrease in the values of $-\overline{uv}$ near the rough wall. It is unlikely to be a consequence of the 'inactive' motion, as one suspects that this is increased in strength in the rough wall layer owing to the considerable increase in the energy in the outer region. This contention is partly supported by the integral length-scale measurements presented in §10.

9. The breakdown of inner layer similarity

A discussion of the various terms in the turbulent energy balance at a station immediately downstream from the step is given below. From these results, and from the observations on mixing length made in §8, it is deduced that the flow in the internal layer is not in a state of energy equilibrium.

A simplified form of the turbulent energy equation for a two-dimensional incompressible mean flow is (Townsend 1956)

$$\left(\underset{\text{advection}}{U \frac{\partial}{\partial x} + V \frac{\partial}{\partial y}} \right) \frac{1}{2} \overline{q^2} - \underset{\text{production}}{\tau \frac{\partial U}{\partial y}} + \underset{\text{diffusion}}{\frac{\partial}{\partial y} (\overline{pv} + \frac{1}{2} \overline{q^2 v})} + \underset{\text{dissipation}}{\epsilon} = 0, \quad (10)$$

where $\overline{q^2} = \overline{u^2} + \overline{v^2} + \overline{w^2}$ and $\tau = -\overline{uv}$. We now assume that $\overline{w^2} = \frac{1}{2}(\overline{u^2} + \overline{v^2})$ so that the total turbulence intensity $\overline{q^2}$ is represented by $\overline{q^2} = \frac{3}{2}(\overline{u^2} + \overline{v^2})$. It is further assumed that \overline{pv} is negligible, so that the diffusion term becomes $\frac{3}{4} \partial(\overline{u^2 v} + \overline{v^3})/\partial y$. The dissipation ϵ is obtained by difference.† The first three terms in the above equation have been evaluated at $x = 4$ in. for $U_1 \delta_s/\nu \simeq 1.9 \times 10^4$ and the results, normalized with respect to δ and U_1 , are plotted in figure 19. The thickness of the internal layer at $x = 4$ in. is approximately 0.4 in., corresponding to a value of y/δ of about 0.20.

The contribution to the production of turbulent energy by the interaction of the normal stresses with the mean velocity gradient in the streamwise direction $(\overline{u^2} - \overline{v^2}) \partial U/\partial x$, neglected in (10), is largest near the wall ($y/\delta < 0.1$) as both $(\overline{u^2} - \overline{v^2})$ and $\partial U/\partial x$ are large in this region. The smooth wall distribution of \overline{uv} $\partial U/\partial y$ shown in figure 19 is that of Klebanoff (1955), obtained at a Reynolds number $U_1 \delta/\nu \simeq 7.8 \times 10^4$ for a zero pressure gradient. Outside the internal layer the two distributions of $\overline{uv} \partial U/\partial y$ are in good agreement. The large values of $\overline{uv} \partial U/\partial y$ inside the internal layer do *not* arise from a transfer of energy flux from the unaffected flow outside the internal layer through the working of the mean flow against the Reynolds shear stress, $\partial(\overline{uv}U)/\partial y$. They are most probably caused by the extraction of the energy from the retarded mean flow in the region near the wall.‡

The relatively large advection in the internal layer arises mostly from $U \partial(\frac{1}{2} \overline{q^2})/\partial x$, for, although $\partial \overline{q^2}/\partial y$ is large and negative over most of the internal layer, V , which is positive, is found to be less than 1% of the local mean velocity U . The plot of $\overline{q^2}/U_1^2$ vs. x (figure 20) shows that, at $x = 4$ in., $\partial \overline{q^2}/\partial x$ increases with distance from the wall, attains a maximum value near $y = 0.3$ in., then decreases

† The curves labelled 'dissipation' in figure 19 thus really include \overline{pv} diffusion.

‡ It is not useful to think in terms of Townsend's (1956) two-layer concept which is applicable to a nearly self-preserving situation. It is more realistic to consider the internal layer as a separate and almost independent boundary layer.

fairly sharply outside the internal layer. The maximum value of the advection occurs near $y/\delta \simeq 0.14$, and represents almost 50% of the value of $\overline{wv} \partial U/\partial y$ there. In the central portion of the boundary layer, the advection is negligibly

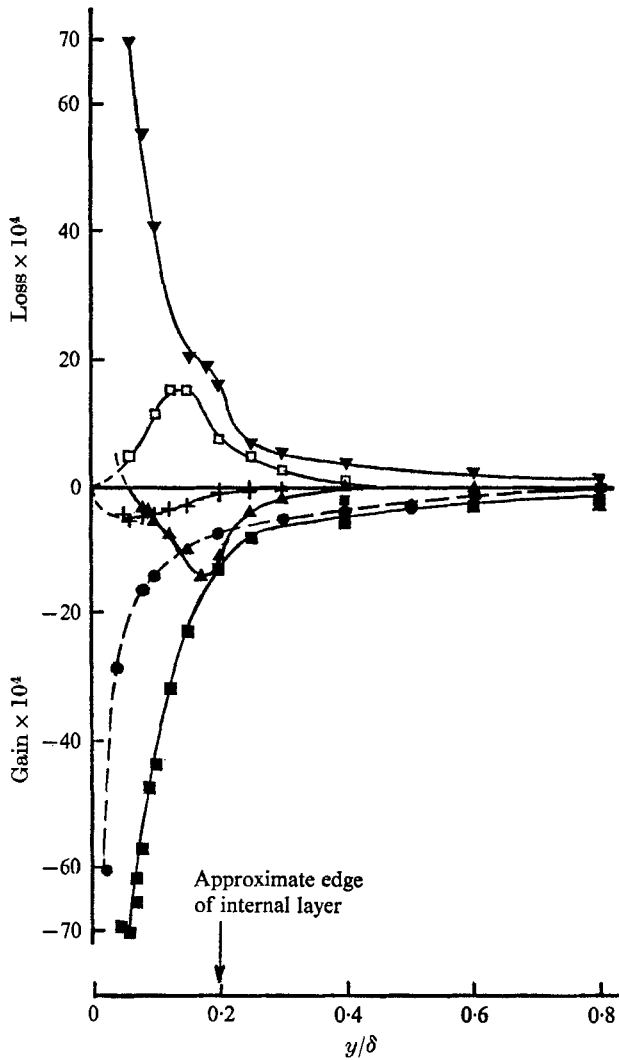


FIGURE 19. Turbulence energy balance at $x = 4$ in. $U_1 \delta_s/\nu \simeq 1.9 \times 10^4$. ■, production by $(\delta U_1^3) \overline{wv} \partial U/\partial y$; ▲, diffusion by $(\delta U_1^3) \partial(\frac{1}{2} \overline{q^2 v})/\partial y$ only; □, advection $(\delta U_1^3) [U \partial(\frac{1}{2} \overline{q^2})/\partial x + V \partial(\frac{1}{2} \overline{q^2})/\partial y]$; +, production by $(\delta U_1^3) (u^2 - v^2) \partial U/\partial x$; ▼, dissipation by difference, ●, Klebanoff (1955) smooth wall production at $U_1 \delta/\nu = 7.8 \times 10^4$.

small. Although no measurements were made near the edge of the boundary layer, it is expected that the advection will rise in this region and remain approximately equal to the diffusion (see e.g. Klebanoff 1955). The details of the energy balance in this region are well documented in the literature, and were not of prime concern in this investigation.

The curves in figure 20 show two main features:

(i) In the range of y from about 0.20 in. to 0.50 in., for a constant value of y , $\overline{q^2}$ rises fairly sharply for small values of x , with its gradient $\partial\overline{q^2}/\partial x$ reaching a maximum at the inflexion point.

(ii) For the smaller values of y , $\overline{q^2}$ appears to overshoot the value finally obtained at the larger values of x .

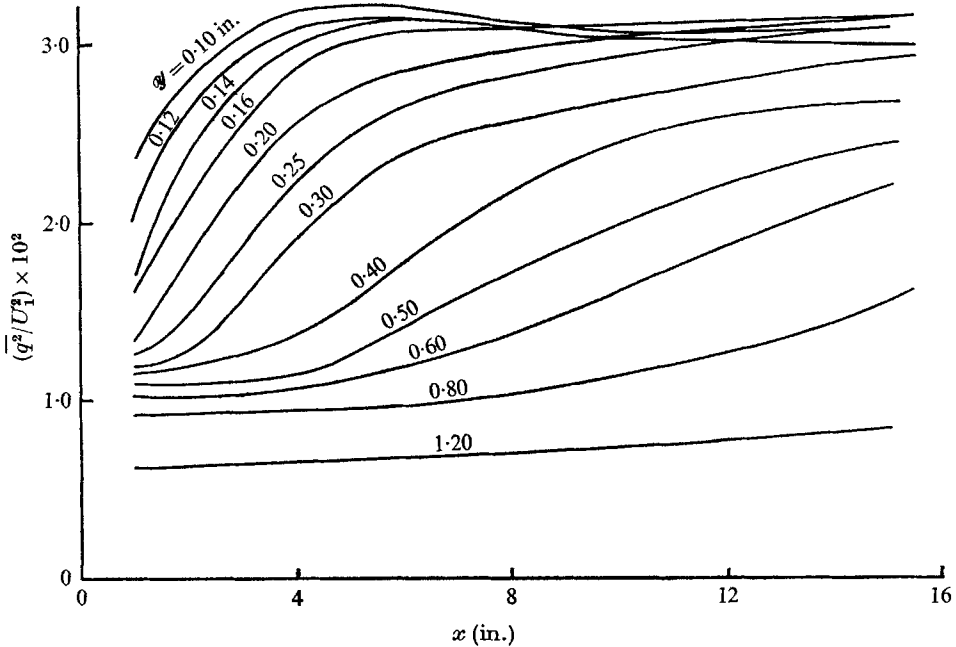


FIGURE 20. Variation of turbulence energy $\overline{q^2}/U_1^2 \simeq 3(\overline{u^2} + \overline{v^2})/2U_1^2$ in region near step change for constant values of y .

Before discussing the diffusion results, some of the main short-comings in the measurement of $\partial(\overline{q^2v})/\partial y$ should be noted.

(i) Because of the non-linearity of the anemometer, the value of $\overline{q^2v}$, particularly in the region near the wall, will be in error. It is unlikely that this error will be large, as the third-order quantity that is most affected by the non-linearity, for a constant temperature anemometer, is $\overline{u^3}$, which does not appear in $\overline{q^2v}$.

(ii) There will be a small error due to phase shifts in the anemometer and in the 1 kHz band limiting filters.

(iii) Although the assumption $\overline{q^2} = \frac{3}{2}(\overline{u^2} + \overline{v^2})$ appears reasonable, no clear assessment can be made of the importance of $\overline{w^2v}$. The measurements of Bradshaw (1967*b*) in a strong adverse pressure gradient show that the absolute value of $\overline{w^2v}$ is larger than that of $\overline{u^2v}$ over the whole thickness of the boundary layer. The measurements of Johnson (1959) in a zero pressure gradient indicate that $\overline{w^2v}$ is not much different from $\overline{v^3}$ over most of the boundary-layer thickness.

(iv) Finally, the data for $\overline{q^2v}$ must be differentiated graphically to obtain the diffusion term $\partial(\overline{q^2v})/\partial y$.

The main feature of the diffusion results in figure 19 is that the gain of energy by the diffusion represents a significant proportion of the total energy gain in the region near the edge of the internal layer. The peak in the diffusion curve at $x = 4$ in. occurs at the value of y at which the $\overline{q^2v}$ distribution (figure 21) exhibits an inflexion. This value of y corresponds fairly closely to the edge of the internal layer. It is interesting to note that the distributions of $\overline{v^3}/(\overline{v^2})^{3/2}$, the skewness of the v -component turbulence intensity, also show a maximum near the edge of the internal layer. The maximum may be interpreted as a maximum in the transport of turbulent energy by the v fluctuations, though it could also be interpreted as a result of a random switching between two different turbulence signals. The distributions of $\overline{v^3}/(\overline{v^2})^{3/2}$ on the smooth wall closely resemble those obtained by Comte-Bellot (1965) for a developing boundary layer on the smooth wall of a two-dimensional channel, and by Johnson (1959) for a self-preserving turbulent boundary layer. The magnitude of the skewness rises fairly sharply as the edge of the boundary layer is approached. This rise is probably caused entirely by the highly intermittent nature of the turbulence in this region. Beyond the edge of the boundary layer, it is expected that the skewness will again decrease fairly rapidly to reach its Gaussian value of zero in the tunnel free stream.

As evidenced by the results of figure 21, there is also an energy gain by diffusion near the edge of the boundary layer. Although this latter gain will be small compared to the gain near the outer edge of the internal layer, it follows that a very large loss of energy by diffusion must occur in the region very close to the wall, so that the area under the diffusion curve is zero. The majority of the $\overline{q^2v}$ distributions over the early part of the roughness indicate that the gradient of $\overline{q^2v}$ near the wall is positive and large.†

However, as the extent over which the positive $\partial(\frac{1}{2}\overline{q^2v})/\partial y$ occurs is small, it is unlikely that this contribution will be of sufficient magnitude to offset the energy gain in the region y/δ greater than about 0.1. The present distributions of $\overline{q^2v}$ on the smooth wall indicate a substantial gain of energy in the outer part of the constant stress region, but, again, the energy loss in the region very close to the wall is by no means large enough to close the diffusion curve. Since the distribution of $\overline{q^2v}$ outside the internal layer at $x = 4$ in. is the same as that on the smooth wall, a large loss of energy by diffusion very near the rough wall appears to be the only solution that will bring about a closure of the diffusion curve. It is likely that there will be an excess of production over dissipation very near the rough wall, which will eventually maintain the high level of turbulence observed in the outer part of the rough wall boundary layer.

Townsend (1961) showed that the major requirements for the existence of an equilibrium layer are that (i) the advection is small, (ii) the dissipation length L_ϵ , defined as $L_\epsilon = \tau^{3/2}/\epsilon$, is directly proportional to y , the relevant length scale‡ in the inner part of the boundary layer.

The advection results of figure 19 clearly indicate that condition (i) is not

† At $y = 0$, $\partial(\frac{1}{2}\overline{q^2v})/\partial y = 0$.

‡ Bradshaw (1967*b*) points out that y is, strictly speaking, the length scale of the active motion only.

satisfied in the outer part of the internal layer. Further, the results of figure 22 show that, in the region occupied by the internal layer, the values of L_e inferred from the present dissipation results are clearly below the line $L_e = \kappa y \dagger$. This agrees with the trend of the mixing length distribution presented in §8. The agreement is not surprising, as the production is very nearly equal to the dissipation over

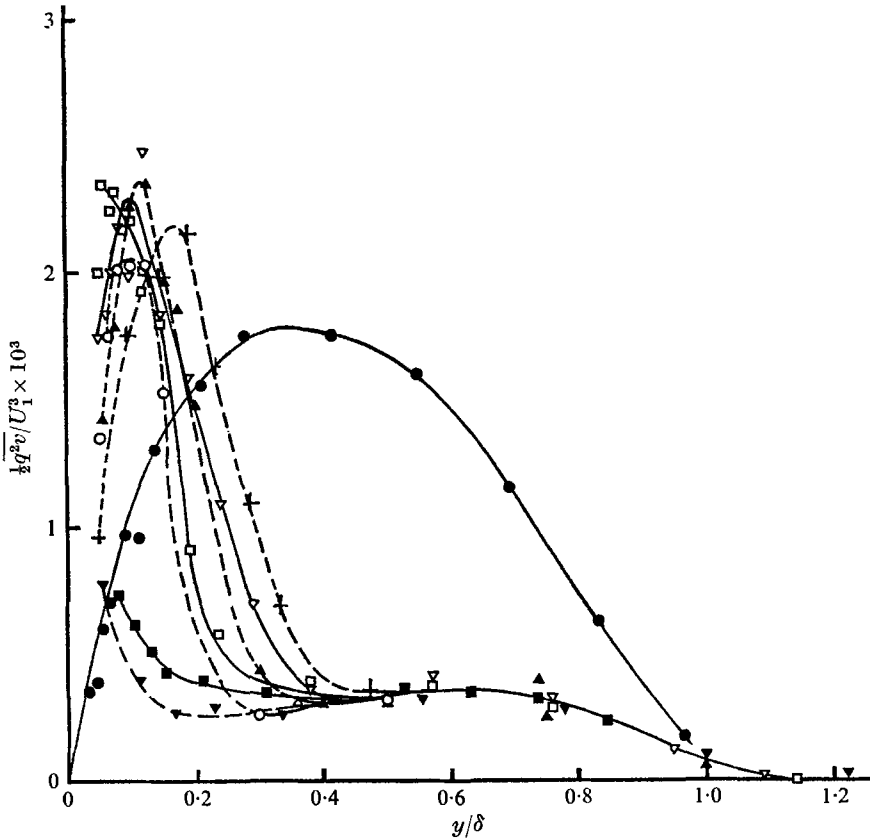


FIGURE 21. Distributions of diffusion energy flux $\frac{1}{2}\overline{q^2v}/U_1^3$. —, $U_1\delta_s/\nu \approx 1.9 \times 10^4$: ■, $x = -4.4$ in.; □, 4; ▽, 6; ●, 46.5. ----, $U_1\delta_s/\nu \approx 3.1 \times 10^4$: ▼, $x = -4$ in.; ○, 3; ▲, 5; +, 8.

most of the internal layer, making L_e very nearly identical with l . It is not unreasonable to expect that the rapidly growing internal layer imposes its own length scale on the flow near the rough wall. If it is assumed that this length scale is given by δ_i , the thickness of the internal layer, then a possible modification to the $L_e = \kappa y$ relation could be $L_e = \kappa y f(y/\delta_i)$. The failure to satisfy the above

† Peterson (1969) points out that there is no theoretical justification for assuming that $l = \kappa y$ is valid in non-equilibrium conditions. He uses some unpublished mixing length results of Plate obtained downstream of a smooth-to-rough step in a wind tunnel, and those of Busch & Panofsky (1968) downstream of a rough-to-smooth step in the atmosphere, to demonstrate his point. The results of Plate indicate a reduction of the mixing length relative to $l = \kappa y$, in agreement with the present finding. The results of Busch & Panofsky indicate an increase in l with respect to κy , in agreement with the results of Antonia & Luxton (1969) for the boundary-layer flow downstream of a rough-to-smooth step.

conditions (i) and (ii) indicates that the concept of inner layer similarity is not applicable for the internal layer flow, and helps to explain the inadequacy of the various calculation methods (see § 1 and § 6) in predicting this flow.

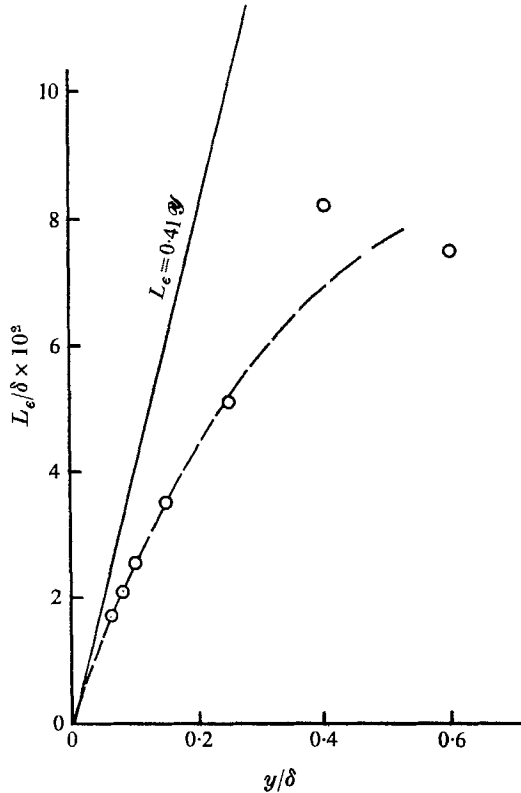


FIGURE 22. Dissipation length scale L_e at $x = 4$ in. derived from turbulent energy balance shown in figure 19.

10. Length scales on the rough wall

In this section the streamwise variation of the longitudinal length scale in the region near the step is discussed. Some measurements have also been made at several stations in the self-preserving rough wall boundary layer and are compared with those obtained on the smooth wall. The length scale variation near the step further suggests a breakdown of inner layer similarity as presented in § 9. The measurements well downstream on the roughness indicate that the structure of the inner layer on the rough wall is different from that on the smooth wall.

10.1. Region near step

The distribution of the longitudinal length scale L in the region near the step is first obtained from the autocorrelation curves at a fixed point. Use is made of Taylor's hypothesis as is defined by

$$L = U \int_0^{t_{\max}} \hat{R}_{uu} dt, \tag{11}$$

where

$$\hat{R}_{uu} = \overline{(u(\mathbf{x})u(\mathbf{x}, t))} / \overline{u^2}. \quad (12)$$

The averaging time for these results was of the order of 30 sec, and the maximum time delay t_{\max} was equal to 30 msec. It was found that, when this value of t_{\max} was reached, the autocorrelation was very nearly zero, or was sometimes slightly negative.

Figure 23 shows the variation of L with x for three constant values of y in the region near the step. Also shown in this figure is the approximate edge of the internal layer. For $y = 0.10$ in., the length scale is reduced by a factor of almost two relative to its value on the smooth wall, and the position at which this reduction first takes place roughly coincides with the edge of the internal layer. As y increases, the reduction becomes less significant. At $y = 0.40$ in., which is just

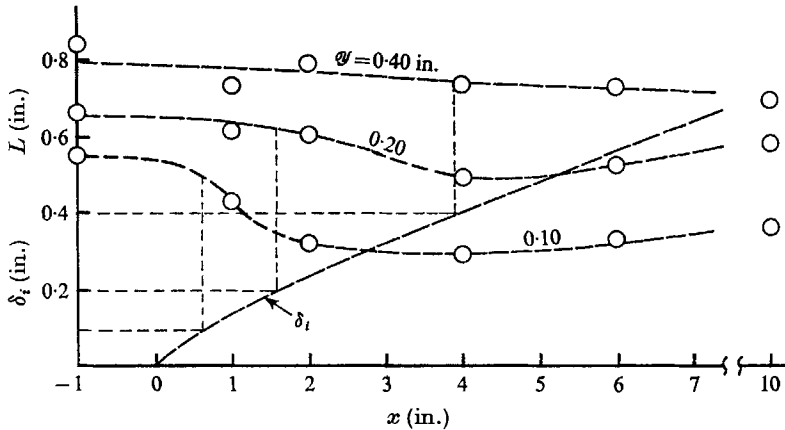


FIGURE 23. Variation of the streamwise integral length scale L with x in the region near the step change. ---, the point at which each distribution enters the internal layer.

outside the logarithmic region of the smooth wall boundary layer, it is expected that L would tend to scale more on the boundary-layer thickness δ . Yet the results show that L is a slowly decreasing function of x , whereas δ increases slightly, if anything, in this range of values of x . This may be due to an 'effect at a distance' by the internal layer, analogous with the concept of inactive motion. The reduction in L near the wall seems to support the reported variation of the mixing length l in the region near the step.

A limited number of two-point space-time correlations have also been measured to verify the trend for L indicated by the fixed point autocorrelations. The normalized longitudinal space correlation coefficient for a zero time delay is defined as

$$\hat{R}_1 = \overline{(u(0)u(r_1))} / (\sqrt{\overline{u^2}(0)} \sqrt{\overline{u^2}(r_1)}), \quad (13)$$

where the normalization is made, for convenience, with respect to the turbulence intensities at the two points that are separated by a distance r_1 , measured in the x direction. The longitudinal length scale L_1 is then given by

$$L_1 = \int_0^\infty \hat{R}_1 dr_1. \quad (14)$$

If the time delay τ is non-zero, the normalized space correlation coefficient then becomes

$$\hat{R}_{1,\tau} = \overline{(u(0,0)u(r_1,\tau))} / (\sqrt{\overline{u^2(0)}}\sqrt{\overline{u^2(r_1)}}). \tag{15}$$

An optimum correlation envelope in space can be obtained by plotting the maximum value of $\hat{R}_{1,\tau}$, denoted here by \hat{R}_{\max} , against r_1 . The time delay (for a given r_1), at which this maximum value occurs, can be used to define a convection velocity U_c for the energy containing eddies, U_c being given by the ratio of r_1

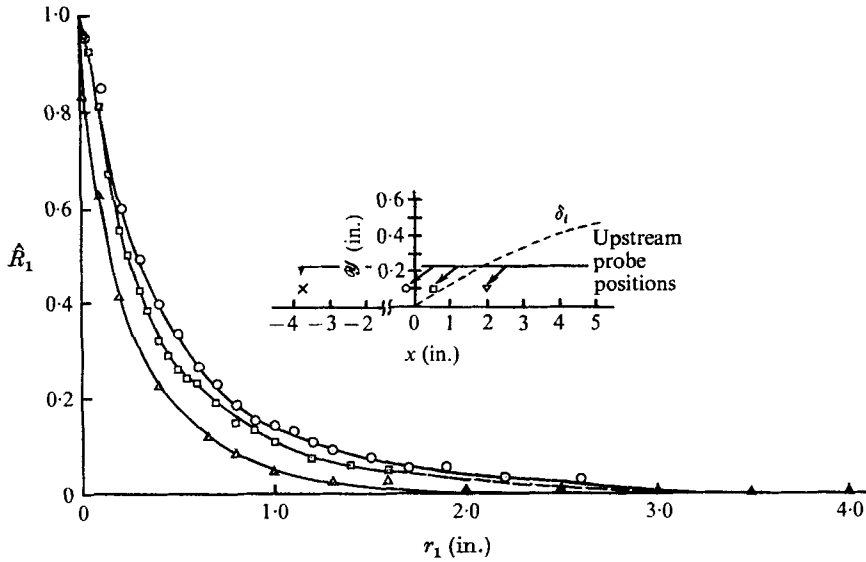


FIGURE 24. Distributions of \hat{R}_1 for three positions of fixed upstream probe at $y = 0.1$ in. \circ , fixed probe at $x = -\frac{3}{8}$ in.; \square , $+\frac{3}{8}$; \triangle , $+2$. Inset shows positions of fixed probe relative to internal layer.

to this time delay. The moving-axis integral length scale L_{\max} , which defines the rate at which the turbulence pattern changes in space, can then be written as

$$L_{\max} = \int_0^{\infty} \hat{R}_{\max} dr_1. \tag{16}$$

The distributions of \hat{R}_1 corresponding to three streamwise positions of the fixed upstream probe for the same value of y in the vicinity of the step are shown in figure 24. It is clear that the extent of the correlation rapidly decreases as the flow responds to the rough wall boundary condition. The length scales L_1 derived from these curves, together with the \hat{R}_1 distribution on the smooth wall at $x = -3.6$ in., are in good agreement with the fixed point autocorrelation results as seen in figure 25. This seems to support the validity of Taylor's hypothesis even in a region where the mean velocity gradient and the turbulence intensities are high.

Calculations of the convection velocity U_c , defined as above, suggest that for small values of the separation distance r_1 , U_c is close to the local velocity U .

As r_1 increases, U_c becomes smaller than U , implying that the large eddies are moving at a slower velocity than the local mean. If the value of the time delay, at which the $R_{1,\tau}$ curve (for a particular value of r_1) is tangent to the optimum correlation envelope in time, had been chosen instead of the present value, the departure of the newly defined convection velocity from the local mean would

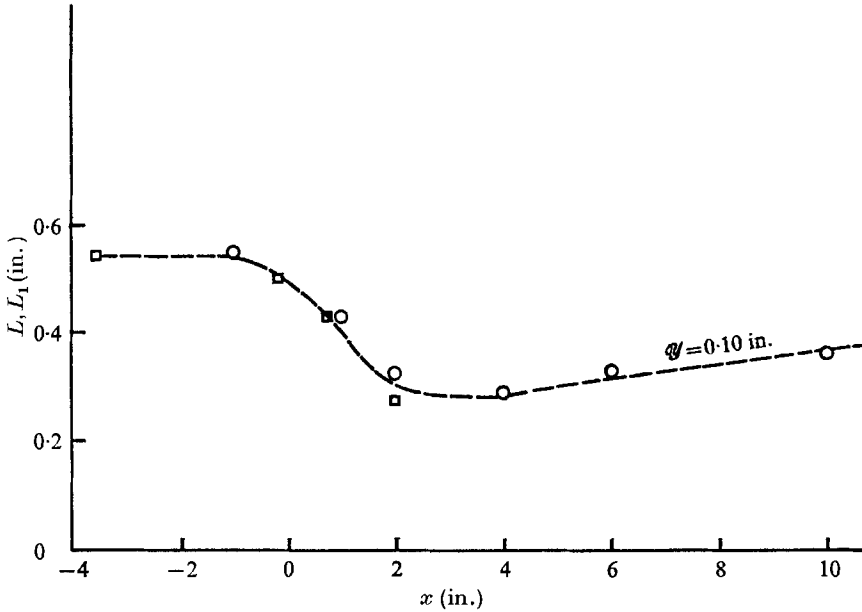


FIGURE 25. Comparison between estimates of streamwise integral length scale from fixed-point autocorrelation (L , \circ) and two-point space-time correlation (L_1 , \square), in region near the step change.

have been somewhat larger. The shortcomings of the above definitions for the convection velocity have been pointed out by Wills (1964), who proposes a more rigorous definition based on the wave-number/phase velocity spectrum, which may be obtained by Fourier transforming the space-time correlations.

The changes in the shape of \hat{R}_{\max} , the optimum correlation envelope in space, along a horizontal plane 0.01 in. distant from the wall are shown in figure 26 for the region near the step. It is seen that the distributions of \hat{R}_{\max} are lowered as the fixed upstream probe moves closer to the edge of the internal layer. It is reasonable to interpret the decrease of \hat{R}_{\max} (with distance r_1) relative to a fixed value of unity, as being due to the rate of change of the turbulence pattern in time or space. The implication is that the eddies which are convected downstream by the mean flow at a velocity nearly equal to the convection velocity are being slowly distorted by the changing rate of strain imposed by the mean flow, or, more specifically, by the rate of generation of 'new' turbulence. The rapid decrease of \hat{R}_{\max} over a short streamwise distance in the region near the step can therefore be attributed to the increased production of turbulent energy inside the internal layer, and consequently to the new and different turbulence structure of the internal layer.

The values of L_{\max} , shown in figure 26, were not obtained from (16), as \hat{R}_{\max} was still relatively large at the largest value of r_1 used. Instead, they were inferred by assuming an exponential fit to the \hat{R}_{\max} curve of the form

$$R_{\max} = \exp(-r_1/L_{\max}).$$

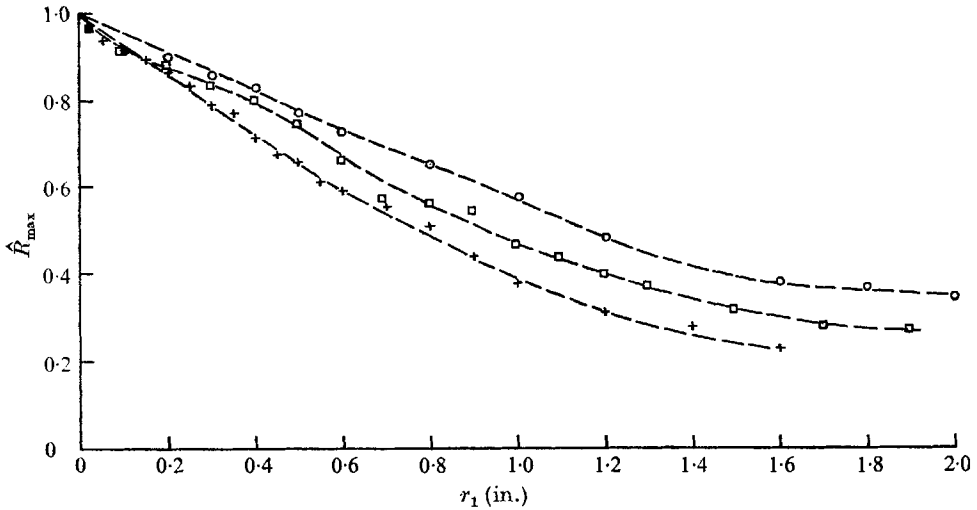


FIGURE 26. Variation of the streamwise space-time correlation at optimum time delay, \hat{R}_{\max} , in the region near the step change at a distance $y = 0.1$ in. from the crests of the roughness. Fixed probe positions are: \circ , $x = -3.6$ in.; \square , -1.2 in.; $+$, $+1.2$ in. The corresponding values of the streamwise moving axis length scale obtained from fitting a curve of the form $R_{\max} = \exp(-r_1/L_{\max})$ to these points are $L_{\max} = 1.66$ in., 1.28 , and 1.03 , respectively.

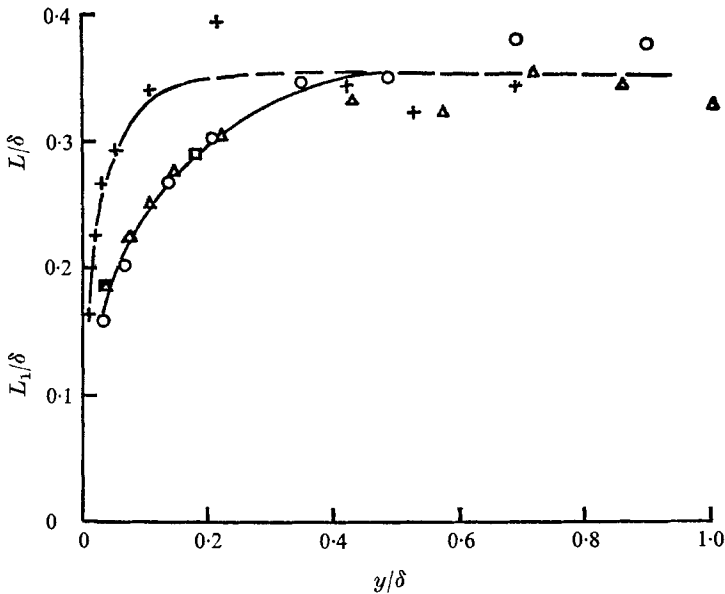


FIGURE 27. Comparison between distributions of longitudinal length scales and rough walls, $U_1 \delta_s/\nu = 1.9 \times 10^4$. Smooth wall: $+$, $x = -1$ in. Rough wall: \triangle , 46.5 ; \circ , 45.2 ; \square , 67.5 . The two points at $x = 67.5$ in. are from two-point correlations (L_1). All other points are from autocorrelations (L).

In figure 27, distributions of the longitudinal length scales across the smooth wall boundary layer are compared with those well downstream on the rough wall. The two values of L_1 indicated for the rough wall were obtained from the zero-time-delay space-correlation curves of figure 28. The curves of \hat{R}_{\max}

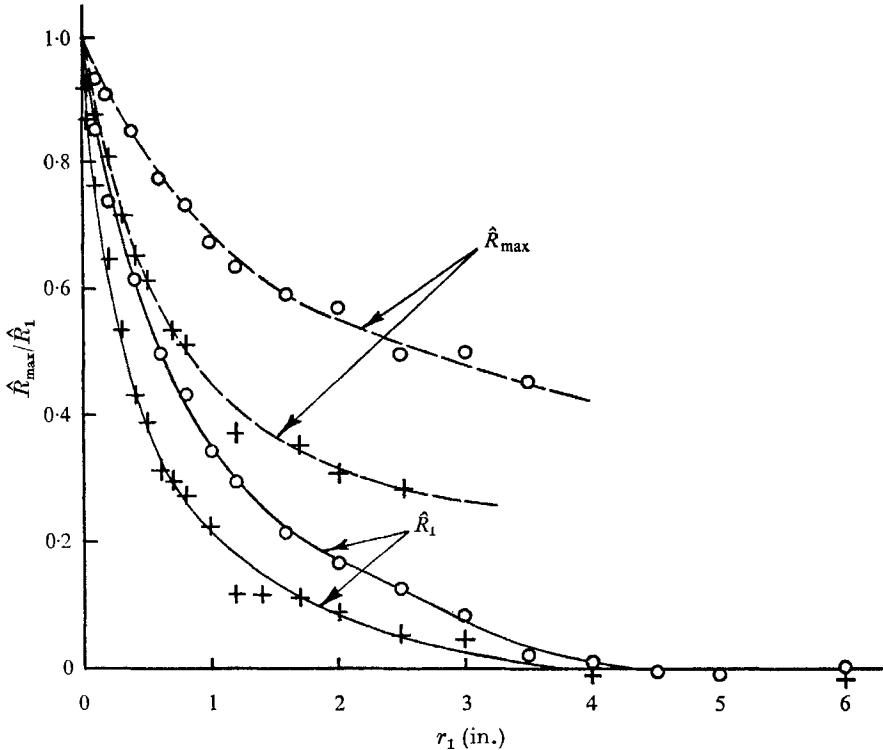


FIGURE 28. Distributions of \hat{R}_1 and \hat{R}_{\max} on rough wall at $x = 67.5$ in. Fixed probe positions are: +, $y = 0.10$ in.; O, 0.60.

also shown in figure 28 tend to indicate a significant increase in L_{\max} across the inner layer on the rough wall. More extensive space-time correlation measurements in the vicinity of a rough wall in a self-preserving boundary layer are needed to allow further comparison of the turbulence structure in the inner region of smooth and rough wall layers. The wave-number phase velocity presentation of these measurements should also provide valuable information about the spread and convection velocity of turbulent energy over a range of wave-numbers.

10.2. Length scales in the self-preserving boundary layer

In figure 27, the distribution of the length scale L across the self-preserving boundary layer on the rough wall is compared with that for an approximately self-preserving smooth wall boundary layer ($x = -1$ in.). The two distributions are in reasonable agreement (taking into account the inevitable experimental scatter) for values of y/δ greater than about 0.3, where it can be assumed that L/δ is approximately constant and equal to about 0.36. This value is in close agreement with the value of 0.37 inferred from spectral measurements by Klebanoff

& Diehl (1951) in a zero-pressure-gradient turbulent boundary layer. Bradshaw & Ferriss (1965) also reported a value of 0.37 in the outer part of a self-preserving boundary layer in an adverse pressure gradient ($U_1 \propto x^{-0.255}$). In the region near the wall ($y/\delta < 0.3$), the values of L/δ over the rough wall are significantly lower than those on the smooth wall. In the latter case, the values of L/δ are progressively reduced, relative to the constant outer value of 0.36, from y/δ of about 0.1 in. to the wall. The decrease in L/δ is much more sudden on the smooth wall than on the rough wall. It was suggested previously that the reduction in L_e in the region near the step was probably caused by the diffusion of turbulence generated directly by the shear layers associated with the individual roughness elements. It is not unreasonable to assume that, at even larger values of x , the dominant length scale for the inner layer turbulence on the rough wall will be a function of the roughness geometry.† It should be pointed out that the observed decrease in length scale near the rough wall is not necessarily incompatible with the previously reported result, that the mixing length l in the region close to the rough wall varies as κy , since l and L need not be directly related near the wall.‡

Some supporting evidence for the observed reduction of L near the rough wall is provided by the space correlation measurements at zero time delay of Chowdhury (1966). These measurements were made at only one point in the inner region of a zero-pressure-gradient boundary layer at a value of y/δ of about 0.023, for both a smooth and a sand-roughened surface. Chowdhury found that the integral length scales in the x and y directions are significantly lower on the rough wall than on the smooth wall, but the length scale in the z direction was higher on the rough wall. Robertson *et al.* (1968) have obtained values of the length scale L from spectral measurements at a few points across the section of a 3 in. diameter sand roughened pipe and of an 8 in. diameter pipe of 'natural' roughness. For a given pipe, reasonably large increases in L are obtained by increasing the Reynolds number, but as the authors themselves state the dependence of L on pipe size and roughness is in need of clarification. No positive statement can be made about the magnitude of L/δ near the rough wall of the pipe as very few measurements are available in this region. Also, since the values of $\Delta U/U_r$ obtained by Robertson *et al.* clearly show that the roughness behaviour was in the transitional régime, the results would probably be of little relevance to the present study. The spectral measurements of Liu *et al.* (1966), made for the same roughness geometry as used here, indicate values of L/δ which are smaller than those on the smooth wall almost throughout the boundary layer, the average value of L/δ in the outer rough wall layer being equal to about 0.30.

11. Summary of conclusions

One of the main points to emerge from the present experimental investigation is that the study of the response of a turbulent boundary layer to a smooth-to-rough change in surface condition is in effect the study of the development of the

† The distribution of $\overline{q^2 v}$ at $x = 46.5$ in. (figure 21) indicates a significant loss of energy by diffusion in the region near the wall.

‡ In the outer region of the self-preserving boundary layer it is found that both l and L are proportional to the boundary-layer thickness δ .

internal layer. The structure of the flow outside the internal layer does not seem to be affected by the new surface condition apart from a small streamline displacement. The readjustment of the boundary layer to the new surface condition takes place fairly rapidly, a distance of less than twenty boundary-layer thicknesses from the start of the roughness being required for the mean flow integral parameters, such as c_f and H , to assume values that are appropriate to the self-preserving boundary layer on the rough wall. The distributions of the turbulence intensities also become approximately self-preserving within a similar distance from the smooth-rough junction.

For the internal layer flow in the region near the step, the following observations are made.

(i) Because of the large production of turbulent energy that occurs near the wall, the level of turbulence intensities is high. In the outer region of the internal layer, the turbulence intensity gradients are also found to be large.

(ii) A significant reduction in the mixing length l relative to the smooth wall distribution κy is observed in the region near the wall. The results of a turbulent energy balance show that the dissipation length scale L_ϵ is nearly equal to l and is, therefore, also reduced. It is further observed that both the zero time delay and the moving-axis integral length scales are considerably decreased near the rough wall. These observations clearly demonstrate the inapplicability of the equilibrium layer concept to the internal layer. The assumption that $L_\epsilon = \kappa y$ needs to be revised before a calculation method can successfully predict the perturbed flow downstream of the step.

(iii) The diffusion of turbulent energy away from the wall plays a dominant part in controlling the growth rate of the internal layer. The energy gain by diffusion has a maximum very near the edge of the internal layer.

(iv) The overshoot of the wall shear stress, inferred from form drag measurements immediately downstream of the step, is not as pronounced as that indicated by the slope of the logarithmic mean velocity profiles.

(v) The mean velocity profiles exhibit a linear trend when plotted in the form U vs. $y^{\frac{1}{2}}$. The edge of the internal layer obtained from these plots appears to grow in much the same way as does the zero-pressure-gradient boundary layer.

The measurements in the self-preserving boundary layer on the rough wall show that the turbulence intensities in the outer layer appear to follow the same self-preserving form as exhibited by the corresponding distributions on a smooth wall. It is suggested that the turbulence structure in the inner layer is strongly influenced by the roughness geometry. The integral length scales are lower than those on the smooth wall. It has also been found that the Reynolds shear stress is not constant, but decreases in the region near the wall. It is tentatively suggested that the missing momentum transport term may be provided by the wavy nature of the streamlines.

The work described in this paper represents part of a programme of research supported by The Australian Research Grants Committee, The Australian Institute of Nuclear Science and Engineering, and The Commonwealth Scientific and Industrial Research Organization.

REFERENCES

- ANTONIA, R. A. & LUXTON, R. E. 1969 *Department of Mechanical Engineering, University of Sydney, Charles Kolling Research Laboratory, T.N.F. 8.*
- ANTONIA, R. A. & LUXTON, R. E. 1971a *Trans. ASME, J. Basic Engng.* **93**, 22.
- ANTONIA, R. A. & LUXTON, R. E. 1971b *Phys. Fluids*, **14**, no. 5.
- BRADLEY, E. F. 1965 Ph.D. Thesis, Australian National University.
- BRADSHAW, P. 1967a *J. Fluid Mech.* **29**, 625.
- BRADSHAW, P. 1967b *J. Fluid Mech.* **30**, 241.
- BRADSHAW, P. & FERRISS, D. H. 1965 N.P.L., *Aero Rept.* 1145.
- BRADSHAW, P., FERRISS, D. H. & ATWELL, N. P. 1967 *J. Fluid Mech.* **28**, 593.
- BUSCH, N. E. & PANOFKY, H. A. 1968 *Quart. J. Roy. Meteor. Soc.* **94**, 132.
- CHANDA, B. 1958 *Colorado State University, Sci. Rept.* 1 CER58BC21.
- CHOWDHURY, S. 1966 *Colorado State University, Tech. Rep.* CER65SC-EJP57.
- CLAUSER, F. H. 1956 *Advan. Appl. Mech.* **4**, 1.
- COMTE-BELLOT, G. 1965 *Publ. Sci. Tech. Min. Air.* 419.
- CORRSIN, S. & KISTLER, A. L. 1954 *NACA T.N.* 3133.
- DOENECKE, J. 1964 *Int. J. Heat Mass Transfer*, **7**, 133.
- ELLIOTT, W. P. 1958 *Trans. Am. Geophys. Union*, **39**, 1048.
- FRASER, D. 1969 *University of Sydney, Department of Mechanical Engineering, Charles Kolling Research Laboratory T.N.F. 9.*
- HAUGEN, R. L. & DHANAK, A. M. 1966 *Trans. ASME, J. Appl. Mech.* 641.
- JACOBS, W. 1939 *Z. angew. Math. Mech.* **19**, 87. Translation 1940, *NACA T.M.* 951.
- JOHNSON, D. S. 1959 *Trans. ASME, J. Appl. Mech.* **26**, 235.
- KLEBANOFF, P. S. 1955 *NACA Rept.* 1247.
- KLEBANOFF, P. S. & DIEHL, F. W. 1951 *NACA T.N.* 2475.
- LIU, C. K., KLINE, S. J. & JOHNSTON, J. P. 1966 *Stanford University, Department of Mechanical Engineering, Rept.* MD-15.
- LUXTON, R. E., SWENSON, G. G. & CHADWICK, B. S. 1967 *The Collection and Processing of Field Data* (ed. E. F. Bradley and O. T. Denmead), p. 497. Interscience.
- LOGAN, E. & JONES, J. B. 1963 *Trans. ASME, J. Basic Engng* **85**, 35.
- MAKITA, H. 1968 M. Eng. Thesis, University of Tokyo.
- MOORE, W. F. 1951 Ph.D. Thesis, State University of Iowa.
- PANOFKY, H. A. & TOWNSEND, A. A. 1964 *Quart. J. Roy. Meteor. Soc.* **90**, 147.
- PERRY, A. E. & JOUBERT, P. N. 1963 *J. Fluid Mech.* **17**, 193.
- PERRY, A. E., SCHOFIELD, W. H. & JOUBERT, P. N. 1969 *J. Fluid Mech.* **37**, 383.
- PETERSON, E. W. 1969 *J. Atmos. Sci.* **26**, 773.
- PLATE, E. J. & HIDY, G. M. 1967 *J. Geophys. Res.* **72**, 4627.
- ROBERTSON, J. M., MARTIN, J. D. & BURKHART, T. H. 1968 *I. & E.C. Fundamentals*, **7**, 253.
- SCHOFIELD, W. H. 1969 Ph.D. Thesis, University of Melbourne.
- TANI, I. 1968 *AFOSR-IFP-Stanford Conference on Computation of Turbulent Boundary Layers*, Stanford University.
- TANI, I., IUCHI, M. & KOMODA, H. 1961 *University of Tokyo, Rept.* 364.
- TAYLOR, P. A. 1969 *Quart. J. Roy. Meteor. Soc.* **95**, 77.
- TAYLOR, R. J. 1962 *J. Fluid Mech.* **13**, 529.
- TOWNSEND, A. A. 1956 *The Structure of Turbulent Shear Flow*. Cambridge University Press.
- TOWNSEND, A. A. 1961 *J. Fluid Mech.* **11**, 97.
- TOWNSEND, A. A. 1965 *J. Fluid Mech.* **22**, 773 and 799.
- TOWNSEND, A. A. 1966 *J. Fluid Mech.* **26**, 255.
- WILLS, J. A. B. 1964 *J. Fluid Mech.* **20**, 417.